Physics – Uspekhi **54** (4) 331 – 349 (2011)

REVIEWS OF TOPICAL PROBLEMS PACS numbers: **63.20. – e**, 64.70.K – , 81.30.Kf

Dynamic model of supersonic martensitic crystal growth

M P Kashchenko, V G Chashchina

DOI: 10.3367/UFNe.0181.201104a.0345

Contents

Abstract. The basic features of martensitic transformations are reviewed using the fcc–bcc (bct) transformation in iron alloys as an example. Supersonic crystal growth is believed to be due to a master wave process initiated by an excited (oscillatory) state that arises in the elastic field of a dislocation. Topics discussed include the mechanism by which nonequilibrium electrons generate (amplify) master waves; the optimum range of parameters for wave generation; the dependence of the transformation onset temperature on the polycrystal size; and the formation of transformation twins due to the coordinated action of relatively short and relatively long wavelength waves. Future research prospects are briefly discussed.

1. Introduction

The phenomenon of martensitic transformation (MT) as a specific variant of the realization of a polymorphic transformation associated with a cooperative mechanism of atomic displacements is attracting the wide attention of researchers. On the one hand, an MT modifies the properties of material and therefore plays an important practical role (it suffices to mention the process of quenching steels). On the other hand, it is quite interesting to construct a physical theory of MTs that would not be limited to fragmentary explanations of separate aspects of this phenomenon but rather would enjoy a high degree of completeness of description of all significant observable properties. It is obvious that such a theory should be based on a clear understanding of the physical nature of the mechanism of control of the structure rearrangement. It is evident that in the case of metals and alloys that represent electron–ion systems, we should first of all understand what features and states of the subsystems are necessary for the development of the MT. The issue is complicated by the fact that in different metallic systems, the MT can occur via different scenarios, which include the differentiation not only of the structures of the initial and final phases but also of the character of the phase transition, whose manifestations in some cases correspond to a limit version of a second-order transition, while in other cases correspond to a clearly pronounced first-order transition. The understanding of both limit cases seems to be important. Nevertheless, the main problems are currently related precisely to the explanation of the MT mechanism in the case of distinctly pronounced first-order transitions.

This is not surprising because such a transition occurs upon a significant deviation from the point of equilibrium of the phases, and the strongly supercooled (or superheated) system is an active medium capable of liberating energy. Consequently, under nonequilibrium conditions, the MT mechanism that ensures the fastest rate of energy liberation may be unrivaled. Detecting such a mechanism requires revising familiar concepts of first-order phase transitions, in particular, revising the problem of the existence of equilibrium (quasi-equilibrium) nuclei of a new phase. It is obvious that in a metallic system, the mechanism of propagation of the fastest relaxation of energy is related to a wave process, and the appearance of waves is related to the initial excited (oscillatory) state of ions, which is maximally efficient for triggering the process of rapid growth of the new phase. In turn, this initial state is localized in those regions of space where, owing to the influence of the elastic fields of defects

M P Kashchenko, V G Chashchina Ural State Forest Engineering University,
ul. Sibirskii Trakt 37, 620100 Ekaterinburg, Russian Federation,
Tel./Fax (7-343) 261 45 51
E-mail: mpk46@mail.ru

Received 17 July 2010, revised 15 September 2010
Uspekhi Fizicheskikh Nauk **181** (4) 345 – 364 (2011)
DOI: 10.3367/UFNr.0181.201104a.0345
Translated by S N Gorin; edited by A M Semikhatov

(e.g., ordinary dislocations), a significant decrease occurs in the interphase energy barrier. This explains the specific character of heterogeneous nucleation. And, finally, the case that is richest in physical contents is where the maintenance of a high (threshold) level of deformations at the front of the control wave process is possible due to the participation of the electronic subsystem.

In coarse blocks, the physically transparent picture described in the preceding paragraph corresponds to a detailed exposition of a new paradigm of MTs, which allows consistently describing a large body of observed facts and removing problems that seemed to be insurmountable for theoretical constructions based on the traditional quasi-equilibrium approach.

The aim of this review is to substantiate the new paradigm of MTs and to demonstrate its efficiency using the example of a reconstructive $\gamma-\alpha$ MT in iron alloys, giving well-deserved credit to the effort of preceding generations of researchers.

2. Specific character of the occurrence of reconstructive martensitic transformations

By definition, reconstructive MTs are cooperative structural transitions between phases whose lattice symmetries are not related by collateral subordination, for example, the transitions from a face-centered cubic (fcc) to a body-centered cubic (bcc) lattice or from a body-centered cubic to a hexagonal close-packed (hcp) lattice. These transformations usually exhibit clearly pronounced signs of first-order transitions. Namely, they are accompanied by a thermal effect and a temperature hysteresis between the forward and reverse transformations. These are typical signatures of any first-order transition, whereas the cooperative character of the crystal lattice rearrangement is a specific property of MTs, which distinguishes them into a separate class of phase transformations.

Below, we consider the variants of MT in iron alloys, namely, $\gamma-\alpha$-(fcc)-(bcc) MT or $\gamma-\alpha$-(fcc)-(fct) MT (fct stands for face-centered tetragonal), for which a large body of experimental data has been accumulated. This transformation was included in the sphere of modern research after the appearance of study [1], where the diffusionless character of the rearrangement with the proximity of neighboring atoms preserved in the initial and final phases has been established.

The morphology of martensite crystals preserves part of the information concerning the cooperative dynamic mechanism of the transformation in the form of a set of macroscopic signs unambiguously connected among themselves [crystallographic orientations of the planar interphase boundaries (habit planes) and macroshear directions, the macroshear magnitude, and the orientation relations between the lattices of coexisting phases]. The pioneering studies concerning precision investigations of morphological signs are [2–4], of which the most complete is that by Greninger and Troiano [4].

Microkinetically, an MT can be defined as an athermal transformation because, first, the rate of transformation (growth) of a separate plate is quite high and is independent of temperature, although the MT itself can occur in a wide temperature range $T \approx (0-10^3)$ K, and, second, the transformed volume increases mainly due to the formation of new crystals rather than due to the growth of the already existing ones. Consequently, the growth occurs, in essence, in the absence of thermal activation, which reveals the meaning of the term 'athermal.'

Macrokinetically, isothermal and athermal MTs can be distinguished. An isothermal transformation can occur at a fixed temperature of the external (with respect to the transformed volume) thermal reservoir; in this case, some optimum temperature exists (depending on the alloy composition) at which the rate of increase in the macroscopic amount of martensite is maximum.

In the case of athermal macrokinetics, the amount of martensite is determined by the degree of overcooling to temperatures less than M_s, whereas the isothermal holding does not lead to an increase in the transformed volume. A limit case of the athermal growth is also observed, namely, a 'burst' MT, in which, during a single 'burst,' a noticeable fraction (several dozen percent) of the entire transformed volume is formed.

A striking feature of the microkinetics, which was noted above, is the high rate of growth of separate crystals. The first measurements [5], which allowed reliably establishing the order of the growth rate ($\sim 10^3$ m s^{-1}), coincident in order of magnitude with the speed of sound, were performed for crystals of lenticular (lens-like) shape with a central completely twinned thin platelike zone (midrib). In addition, it was supposed in [5] that the anomalous increase in the electric resistance at the initial stage of crystal growth (in contrast to the expected monotonic decrease) indicates the two-stage character of the formation of a martensite plate. In the experiments in [6], the rate of martensite growth is comparable to the supersonic value 6.6×10^3 m s^{-1} characteristic of longitudinal waves. In addition, it was noted in [6] that this conclusion agrees with the results obtained in [5] if the observed size of the first coarse martensite crystals (which coincides with the grain diameter) is divided by the time of the anomalous increase in the resistance. This means that the supersonic growth rate should be related to the first stage of the fast formation of the midrib. The two-stage character of the formation of lenticular crystals is currently beyond dispute. An analogous conclusion follows, for instance, from experiments on the effect of magnetic fields on the MT [7]. Thus, *there are grounds to assume that the rate of the formation of platelike crystals* (*or of the central zone of lenticular crystals*) *is supersonic* (*with respect to longitudinal waves*).

This conclusion has a fundamental importance because, based on quite general physical concepts, it allows performing a selection among various scientific paradigms used in the interpretation of the phenomenon of the martensitic reaction in alloys of transition metals, i.e., performing a selection of physical concepts consistent with a high (supersonic) growth rate.

3. Problems with the theory of reconstructive martensitic transformations

Historically, the start of the rapid development of the theory of MTs is due to Bain (see, e.g., [8]). Because an fcc lattice can be considered a bct lattice with the tetragonality $t = \sqrt{2}$, Bain noted [8] the possibility of a deformation-induced transformation of the fcc lattice into a bcc lattice (Fig. 1) through a 20% compression along one of the $\langle 001\rangle_\gamma$ axes and synchronous tensions by approximately 13% along a pair of orthogonal axes, e.g., $\langle 100\rangle_\gamma$ and $\langle 010\rangle_\gamma$ (or $\langle 110\rangle_\gamma$ and $\langle -110\rangle_\gamma$).

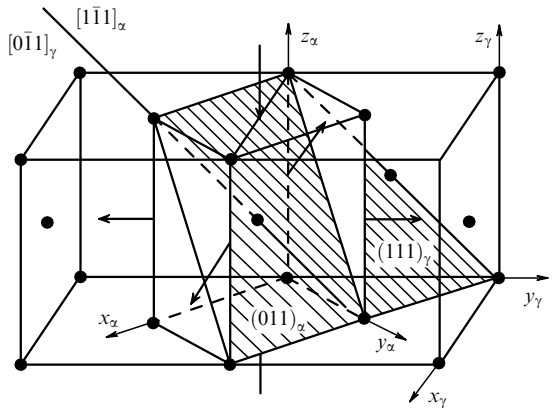

Figure 1. Scheme illustrating the Bain deformation and crystallographic correspondence of the planes and directions [9]. The directions of compression and tension are shown by solid arrows; the close-packed plane $(111)_\gamma||(011)\alpha$ is hatched.

A noticeable success in the treatment of morphological signs of low-temperature ($\{259\}_\gamma - \{3\ 10\ 15\}_\gamma$ habits) martensite was achieved when using a crystallographic approach, which was sufficiently completely reflected in [10–13]. In this approach, the MT is associated with the deformation of the initial phase, which has a macroscopic invariant plane, the habit plane. The lattice deformation is described either in a shear scheme supplemented by dilatations or in the scheme of the Bain deformation with subsequent rotations, which ensure the fulfillment of the orientation relations.

Because the Bain deformation is not a deformation with an invariant plane (for such a deformation, one of the principal components vanishes and the other two components have different signs), an additional deformation (not changing the lattice symmetry) is used to ensure that the total macrodeformation of the transformed region is reduced to the deformation with an invariant plane. In particular, for low-temperature martensite, twinning was selected as the additional deformation (see the scheme in Fig. 2c).

One of the disadvantages of this approach is the absence of a physical substantiation of the choice of specific deformation mechanisms. In addition, these theories do not explain changes in the crystallographic features of the transformation, depending on the changes in the composition or temperature [14].

As regards the thermodynamic approach to the theory of MTs, we note that the preference is naturally given to a phase with the lowest Gibbs free energy $G(P, T)$, which is defined by [15]

$$G(P, T) = H - TS = U + PV - TS, \tag{1}$$

where H, U, S, and V are the specific values (calculated per 1 mol of a substance) of the enthalpy, internal energy, entropy, and volume, respectively, and P is the pressure.

The calculation of thermodynamic (macroscopic) values in (1) in terms of the quantum statistical approach is a sufficiently complex problem because the values of G for different phases differ only insignificantly and no radical simplifications can be used in calculations. Nevertheless, taking all significant factors (including the magnetic properties of the phases) into account allows substantiating the observed polymorphism in pure iron and its alloys. Not

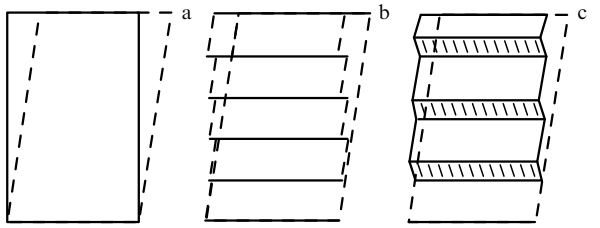

Figure 2. Recovery of the shape of the transformed region by an additional deformation [9]: (a) the proper transformation deformation; (b) the recovery of shape by slipping; and (c) the recovery of shape by twinning.

considering the problem of phase stability in more detail, we assume below that the answer to this question is known.

The use of thermodynamics for considering some features of the morphology of products of an MT, which is based [16] on taking the energy of internal stresses into account in the system of coexisting γ and α phases, assumes that the formation of the final structure reflects the tendency of the system to a state with a minimum elastic energy of internal stresses.

In the case of a supersonic velocity of crystal growth, it is expedient at once to concentrate attention on the dynamic mechanism of controlling crystal growth and to interpret the formation of vast platelike regions as a process (developing in space and time) of the loss of lattice stability in the initial phase. We also emphasize that the region that loses its stability during the transition to a new stable (at least, metastable) state does not have the elastic reaction characteristic of the stable state of the new phase. It is clear that the dynamic mechanism of control is of the wave kind, and that the use of mobile dislocations is excluded. We also recall that in the continuum description [17], the limit velocity for dislocations is the velocity of transverse elastic waves, while in the atomistic description, the maintenance of a high velocity of dislocation motion under the conditions of intensive loss for the emission of elastic waves (an analog of the Vavilov–Cherenkov effect) would require too high a level of stresses. Indeed, according to [18], the stress σ required for the maintenance of a velocity $v > c_t$ can be estimated as

$$\sigma \approx \left(\frac{v^2}{c_t^2} - 1\right) \frac{\mu b}{2\pi a}, \tag{2}$$

where μ is the shear modulus, b is the Burgers vector, and a is the spacing between the sip planes. It follows from (2) with $v \approx 2c_t$ and $b \approx a$ that the value of σ exceeds the theoretical ultimate strength $\sigma_{max} \approx 0.1\mu$, and therefore makes no physical sense. This means that the motion of the interphase boundary should be regarded as a nonlinear wave process.

Particularly acute is the problem of the formation of a regular structure of transformation twins (*with an alternation of two orientations of the Bain compression axes* [9]), *whose mechanism should be consistent with the supersonic velocity of crystal growth.*

Thus, the existence of a high growth rate is a criterion that can serve for the selection of a concrete paradigm of the MT. The heart of such a paradigm amounts to the identification of the dynamic structure of the interphase region at the stage of rapid growth, which allows understanding the crystal growth control mechanism [19, 20]. It is also evident that the dynamic mechanism of supersonic growth is inconsistent with the paradigm based on the concept of the existence of thermodynamically equilibrium (or quasi-equilibrium) nuclei of the

new phase. *It is also no coincidence that the search for such nuclei yielded no results and thereby generated the problem of 'unobservable nuclei.' Therefore, the basic concepts of the mechanism of supersonic growth of a martensite crystal should be connected with a new description of the initial stage of this process.*

The understanding of the importance of kinetic factors in the development of an MT was reflected in several review papers (see, e.g., [21, 22]). The attention is traditionally focused on the analysis of magnitudes of energy barriers that should be overcome with this type of growth, as well as on estimations of the thermodynamic driving force of the transformation and of the contributions from relaxation processes. On the whole, the concept of relaxation as a variant of switching between two states separated by an energy barrier is quite acceptable. The treatments based on the use of a Ginzburg–Landau functional [23] and its generalizations applied to different models (differing in spatial dimensionalities and types of structural rearrangements) (see, e.g., [24–34]) reduce the problem of the growth mechanism to the consideration of a model of a phase boundary and to the investigation of its mobility.

Of great importance is the issue of the stability of the austenite lattice at the temperature M_s, which is connected with the problem of the existence of a temperature T_c corresponding to the absolute loss of stability of the initial phase. Indeed, the existence of a temperature $T_c > 0$ at which a lattice containing no defects becomes unstable with respect to infinitely small fluctuations would mean the unavoidable occurrence of an MT upon cooling. However, for alloys with both isothermal transformation kinetics [35] and with athermal kinetics [36], the MT can be suppressed by cooling to temperatures below M_f (which specifies the lower boundary of the interval of temperatures for the realization of the MT for the alloy of a given composition, $T_0 > M_s > M_f$) and then induced by warming. The absence of T_c and, consequently, the relative stability of the fcc lattice at the M_s temperature, pose the problem of the magnitude of the energy barrier that should be overcome by the system in the process of nucleation and growth. This problem is connected with the question of the large magnitude of the overcooling, $T_0 - M_s \approx 200$ K, which was formulated in [37, 38]. *The heart of the problem lies in the significant difference between the estimation of the overcooling* $\Delta T = T_0 - M_s \approx 45$ K *necessary for the compensation of the energy expenditures* ($E_e \approx 50$ cal mol^{-1}) *for the external work in the process of MT and the magnitude of* $T_0 - M_s$. One acceptable explanation [39] amounts to the fact that the kinetics of the process is controlled by the rate of the transition of the system through the energy barrier related to the formation of centers of the new phase, because the growth of martensite crystals occurs almost instantaneously and, consequently, the degree of overcooling $T_0 - M_s$ can be determined not only by the thermodynamic but also by the kinetic characteristics of the process.

The unobservability of the nuclei and their high growth rate indicate the nonclassical character of the start of growth of a martensite crystal caused by the generation of an initial excited state. The thermal effect of the transformation can then be interpreted [19, 20, 40] as a result of the distribution of the energy E of atomic oscillations near the new equilibrium positions with a small number of preferred directions of polarization over all $3N_N$ oscillation modes of the excited region with the number of atoms N_N. We estimate E assuming that the longitudinal oscillations polarized in two directions (we let x and y denote them) are mainly excited. The contribution from one mode, with a wave vector q_i ($i = x, y$), to the energy E can be written as

$$E_{q_i} = \frac{1}{2} M\omega_{q_i}^2 |u_{q_i}|^2 N_N , \tag{3}$$

where M is the mass of an atom and ω and u are the cyclic frequency and the amplitude of the oscillations. We note that the relative deformation ε associated with oscillations is characterized by the maximum value

$$\varepsilon_m \approx \frac{2u}{\lambda/2} = \frac{2uq}{\pi} , \tag{4}$$

where $\lambda/2$ is the spacing between two planes that vibrate in antiphase (λ is the wavelength). Assuming ε to be equal for all q_i, making substitution $\omega_{q_i} \to \omega_{q_i} = cq_i$, where c is the speed of sound, and recalling that q_x and q_y take $N_{N_x} \approx N_{N_y} \approx 2r_N/a$ values (r_N is the radius of the initial excited state and a is the lattice constant), we use (3) and (4) to obtain

$$E = \sum_{i,\,q_i} E_{q_i} \approx \frac{\pi^2}{2a} r_N N_N M c^2 \varepsilon_m^2 . \tag{5}$$

The estimation of ε by the time instant $t = t_N$ at which the initial excited state is formed can be obtained assuming that

$$\frac{E}{N_N M} \approx \frac{\pi^2}{2a} r_N c^2 \varepsilon_m^2 \approx Q , \tag{6}$$

where Q is the specific (per unit mass) transformation heat. For $Q \approx 4 \times 10^4$ J kg^{-1} (alloy N30 [41]), $r_N \approx 10^{-7}$ m, $a \approx 3 \times 10^{-10}$ m, and $c = 5 \times 10^3$ m s^{-1}, we find from (6) that $\varepsilon_m \approx 10^{-3}$. Hence, at least for most long-lived modes with the quasimomentum $q \approx q_{min} \approx \pi r_N^{-1}$, which by the instant $t = t_N$ is final for the stage of the formation of the initial excited state and is simultaneously initial for the stage of growth, we can expect that the threshold deformation is $\varepsilon_{th} \leqslant \varepsilon_m$. It is useful to compare this result with the data in [9, 42] concerning the effect of external stresses on the MT. The grounds for the comparison, for example, with the data on the effect of tensile stresses, are evident if we note that the quantity $\lambda/2$ in (4) plays the role of the initial length of the sample l and the amplitude u plays the role of the absolute elongation Δl, and if we also take into account that $\lambda_{max} = 2\pi/q_{min} \approx 10^{-7} - 10^{-6}$ m is many times greater than the lattice parameter a. An interesting bit of information is the fact that a temperature M_{elast} [42] exists near M_s ($M_{elast} - M_s \approx 35 - 40$ K) such that the MT at temperatures T in the range $M_s < T < M_{elast}$ is caused by external elastic stresses σ_m. Because the elastic deformation corresponds to $\varepsilon \leqslant 10^{-3}$ in the stress–strain diagram, we conclude that the condition $\varepsilon_{th} \leqslant 10^{-3}$ is acceptable for the threshold deformation.

Consequently, in the model of the formation of the initial excited state capable of ensuring rapid growth, the large overcooling $T_0 - M_s$ is interpreted as a necessary condition for the excitation of oscillations with finite amplitudes (and frequencies) ensuring the inequality $\varepsilon \approx \varepsilon_{th} \leqslant 10^{-3}$ corresponding to the lattice stability criterion of the γ phase at the M_s point. This conclusion allows lifting the apparent contradiction between the requirement of the metastable stability of austenite at the M_s point, which presumes a finite magnitude of the interphase barrier, and the virtually

temperature-independent growth rate of martensite (in a wide temperature range), which indicates a barrierless (over-barrier) character of motion. Indeed, the initial excited state with vibrations that ensure deformations exceeding the threshold level can induce a wave process, violating the lattice stability, with a rate that depends only on the elastic properties of austenite.

The wave approach applied to the problem of martensite growth was first formulated in a distinct form in [43]. Without using concrete values of the velocities, the authors of [43] suggested a scheme of two sequential deformation waves. The first wave propagates from a small disklike nucleus in radial directions, causing a uniform deformation of a plate-like region whose surface (habit plane) coincides with the invariant plane. When the stresses caused by the deformation from the first wave reach a certain critical value (supposedly, yield stress) in the direction perpendicular to the habit plane, the propagation of a second wave starts, which leads to a shear nonuniform deformation (uniform only macroscopically), completing the process of the formation of a martensite plate.

The ideology suggested in [43] is mainly retained in [44]. It was additionally postulated there that a wave propagating in a radial direction is longitudinal, causing an MT in the central zone (in the midrib zone). The transformed regions of the midrib play the role of second-order nucleation centers for the excitation of a transverse transformation wave (propagating in the direction perpendicular to the habit plane). But the description of the midrib formation mechanism, which has an internal twin structure and plays the leading role in the formation of a lenticular crystal, just as the treatment of rich morphological signatures of an MT, was absent in [43, 44].

If we do not accentuate the problem of the role of dislocations in the process of the formation and propagation of the interphase boundary, the motion of the boundary in the above-considered models can be interpreted uniformly as the propagation of a solitary front, which is also called the switching wave (see, e.g., [45]) — a step-like excitation, to the left and to the right of which different values of the deformation $\varepsilon_{\alpha,\gamma}$ are realized, characteristic of the γ and α phases. The basis for the description of such a process can be a quasilinear parabolic equation (a nonlinear diffusion equation).

We now consider studies that focus on the role of hyperbolic waves in MTs. In the general case, these waves satisfy nonlinear equations that arise from a hyperbolic linear equation (classical wave equation with second derivatives with respect to the coordinates and time), for which the sinusoidal waves are the fundamental solution. Such waves can easily be represented as ensembles of phonons, which allows using microscopic models that are well developed in solid-state physics by establishing connections between microscopic and macroscopic descriptions.

In [46], the author stated the validity of the description of MTs on the basis of wave positions. In view of the unobservability of the static nuclei of martensite, it was suggested that the stages of the nucleation and growth not be distinguished and the kinetics of any MTs be regarded as the 'burst' kind (assuming that the slow growth of an isolated crystal occurs as a result of a sequence of rapid microbursts separated by long pauses). In addition, specific features of the martensite structure were to be regarded as a consequence of the action of combinations of lattice modes propagating with the velocities of elastic waves.

The first attempt to relate the activation of an athermal (burst) MT in iron alloys to the stimulated radiation of phonons (effect of a phonon maser) realized upon overcooling to temperatures substantially lower than the phase equilibrium temperature T_0 was undertaken in [47]. There, the optimum frequency was assumed to be that of Debye phonons $\nu_{AM} \approx 10^{13}$ Hz with the energy $h\nu_{AM}$ that was assumed to be equal to the difference in the specific (per atom) free energies $G_A - G_M$ of the metastable austenite (G_A) and stable martensite (G_M). Atoms that execute a coordinated (cooperative) jump from an energy level G_A to the level G_M are assumed to be a radiating system. The zigzag structure exhibited by a group of relatively fine crystals that are formed between two coarse plates was regarded in [47] as a consequence of repeated reflections of stimulated phonon radiation from coarse plates. Figure 3a schematically shows the observed zigzag structure (in metallographic work, more usual names are lightning and framework structures); Fig. 3b displays the Kaiser scheme (solid lines).

A characteristic feature of this structure is the existence of two sets of plates: any two plates of the same set are parallel; pairs of plates of different sets meet at an acute angle. We note, however, that in the case of nonparallel coarse plates, it is impossible to construct two such sets of plates based on the law of reflection. Both the interpretation of the radiating system and the choice of the frequency of radiation seem to be doubtful. The difficulty in determining the wave generation mechanism remained unsurmounted in [48], where the author attempted to draw an analogy between a laser and an MT and to give a phenomenological description of a wave of transverse displacements.

Investigations of the temperature dependence of elastic moduli [50, 51], just as of the dispersion curves of the phonon spectrum [50–53], before the $\gamma - \alpha$ MT show the absence of even a tendency to lose stability in the majority of cases. The anomalous temperature dependence (observed in [50]) of the elastic moduli in the Fe–Ni system (with more than 30% Ni), in which a ferromagnetic ordering is observed at $T > M_s$, should more likely be related to the effect of this ordering [54, 55] than to the manifestation of the tendency toward lattice instability; in other words, we are dealing here with 'normal' elastic moduli, but with those of a ferromagnetic system. In other words, the austenite lattice preserves stability with respect to separate small-amplitude phonon modes. Nevertheless, the investigations of the pretransition state (see, e.g., [56–61]) are interesting for constructing a dynamic model of MTs, just as the symmetry analysis is interesting for the determination and use of order parameters [57, 62].

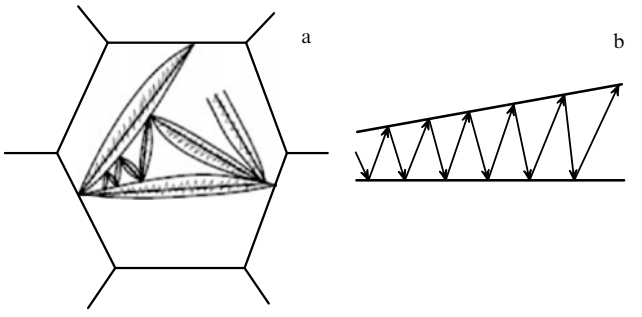

Figure 3. Framework structure of martensite crystals: (a) a set of lenticular twinned crystals in a realistic scheme [49]; and (b) an idealized scheme of a multiple reflection of stimulated phonons [47].

Among many studies indicating a heterogeneous character of nucleation, we note the experiments in [63] with small particles (with a diameter greater than 10^{-6} m), which have convincingly demonstrated that at the equal size of particles, the MT is by no means developed in all of them in the process of cooling. This supports the assumption that martensite nucleates in only certain preferred centers. The same conclusion follows from the facts observed upon thermocycling, where both the initial and repeated growth of martensite crystals typically occurs at the same sites. Some results of electron-microscopic observations indicate the participation of dislocations in the processes of martensite nucleation.

4. Initial excited state and the model of the control wave process

Although the list of significant facts and problems is not exhausted, the information presented in Sections 2 and 3 is sufficient to formulate a model that optimally combines the simplicity of the description with the completeness of the interpretation of the rich totality of the observed features of MTs.

Taking into account that the threshold deformation ε_{th} belongs to the elastic range, it is natural to assume that a defect with its elastic field decreases the interphase energy barrier, breaks the initial symmetry of the lattice, and singles out regions in which the loss of stability in approaching the M_{s} temperature leads to the appearance of an initial excited state. Determining the shape, size, crystallographic orientation, character of excitation, and level of energy of such states gives very important information for the understanding of the subsequent growth of a martensite crystal.

The results of calculations (see, e.g., [64–74]) indicate that even a separate dislocation typical of a given symmetry of the lattice creates an elastic field that is favorable for the appearance of an initial excited state. Figure 4 shows that at a certain distance r from a dislocation line, a region can always be distinguished in the shape of an elongated rectangular parallelepiped with transverse dimensions $d_{1,2}$ constructed on orthogonal eigenvectors $\boldsymbol{\xi}_i$ of the tensor of elastic deformations. In this case, there are angular ranges $\Delta\Theta$ (near a certain value Θ_0) with opposite-sign deformations along the $\xi_{1,2}$ axes that are orthogonal to the larger edge ξ_3, along which the deformation is close to zero. The corresponding principal values of the deformation tensor in the nucleation region satisfy the condition for plane deformation with a pair of invariant (weakly distorted) planes, i.e.,

$$\varepsilon_1 > 0\,, \quad \varepsilon_2 < 0\,, \quad \varepsilon_3 \approx 0\,, \tag{7}$$

and, moreover, the values ε_1 and $|\varepsilon_2|$ are close to the maximum values $\varepsilon_1(\Theta_0)$ and $|\varepsilon_2(\Theta_0)|$ (the extrema are sought with respect to the angular variable Θ at a certain fixed distance r from the dislocation line). Consequently, in the nucleation region, the elastic field of the defect maximally decreases the energy barrier for the onset of plane deformation with an invariant (at $\varepsilon_3 = 0$) or weakly distorted (at $\varepsilon_3 \approx 0$) plane.

It is therefore assumed that the role of the volume element in which an ensemble of atoms passes through the energy barrier (with the liberation of energy and excitation of oscillations) is played by a three-dimensional cell in the form of an elongated rectangular parallelepiped. The faces of this parallelepiped vibrate pairwise in antiphase, stimulating a

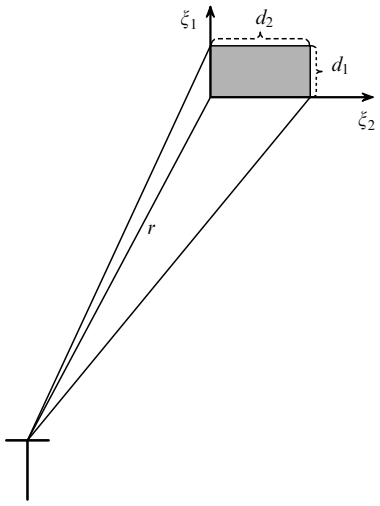

Figure 4. Region suitable for the localization of the initial excited state in the elastic field of a separate dislocation (the ξ_3 axis is orthogonal to the figure plane).

threshold tension–compression deformation in mutually orthogonal directions coinciding with the propagation directions of wave beams radiated by the vibrating parallelepiped. The lattice sequentially loses stability, forming a platelike region at the sites where wave beams with an atomic-displacement field favorable for the realization of the threshold deformation are superposed (Fig. 5).

The formation of a platelike prototype of a martensite crystal can naturally be interpreted as a movement of the parallelepiped with a velocity $\mathbf{v}$ that is the vector sum of velocities $\mathbf{v}_1$ and $\mathbf{v}_2$ of the wave beams. Because the liberation of energy necessary for the autocatalytic feed-up of the wave occurs only in the volume that underwent the threshold deformation, it is precisely the supersonic velocity $\mathbf{v}$ that becomes the true rate of crystal growth.

Consequently, the synthesis of the concepts of heterogeneous nucleation and wave growth can be achieved if we assume that the normals $\mathbf{n}_1$ and $\mathbf{n}_2$ of the wave beams describing the tensile ($\varepsilon_1 > 0$) and compression ($\varepsilon_2 < 0$) deformations in the superposition region are collinear to the eigenvectors $\boldsymbol{\xi}_i$ ($i = 1, 2$) of the deformation tensor of the

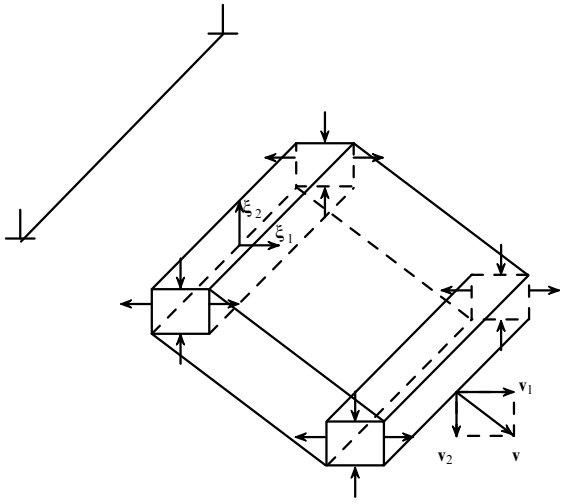

Figure 5. Wave model of controlling growth of a martensite crystal (the segment bounded by the symbols $\perp$ corresponds to a dislocation line).

elastic field of the defect in the nucleation region:

$$\mathbf{n}_1 || \boldsymbol{\xi}_1, \quad \mathbf{n}_2 || \boldsymbol{\xi}_2, \quad \mathbf{n}_1 \perp \mathbf{n}_2 \quad |\mathbf{n}_i| = |\boldsymbol{\xi}_i| = 1 . \tag{8}$$

This means that the control wave process (CWP) inherits the information concerning the directions of the principal deformation axes. It can be easily shown [19, 20, 75–78] that the normal $\mathbf{N}_w$ to the habit plane, which is related to the propagation of the CWP, is specified by the kinematic relation

$$\mathbf{N}_w || \mathbf{n}_2 - \mathbf{n}_1 \varkappa, \quad \varkappa = \frac{v_2}{v_1} , \tag{9}$$

where v_1 and v_2 are the moduli of the wave propagation velocities in the directions $\mathbf{n}_1$ and $\mathbf{n}_2$. On the other hand, in the case of plane homogeneous tensile–compressive deformation, the normals to the invariant planes are written as

$$\mathbf{N}_d = \boldsymbol{\xi}_2 \pm k \boldsymbol{\xi}_1 , \tag{10}$$

$$k = \frac{1 - |\varepsilon_2|}{1 + \varepsilon_1} \left(\frac{\varepsilon_1}{|\varepsilon_2|} \frac{2 + \varepsilon_1}{2 - |\varepsilon_2|} \right)^{1/2} . \tag{11}$$

Because the CWP implements deformation with an invariant plane, it is natural to assume that the coincidence of the kinematic and dynamic descriptions of the habit plane occurs in the propagation of the CWP; i.e., formulas (9) and (10) describe the same habit if the values of ε_i in (11) correspond to the threshold values. Using (8), we then obtain the important condition

$$\varkappa = k , \tag{12}$$

which determines the relation between the deformations and velocities of waves existing in the propagation of the CWP.

The smallness of the threshold deformations ε_{th} allows representing condition (12) in the form

$$\varkappa = \frac{v_2}{v_1} = k \approx \sqrt{\frac{\varepsilon_1}{|\varepsilon_2|}} , \tag{13}$$

where the velocities v_2 and v_1 can be calculated from the Christoffel equation [79] using the elasticity moduli of the initial crystal lattice (preferably, at the M_s temperature). Such an algorithm allows identifying the dislocation centers of nucleation of concrete martensite crystals.

In view of the fundamental importance of the concepts concerning the character of the initial excited state, experiments with a physical simulation of the initial excited state by a laser pulse with the duration of 20 ps and a linear shape of the trace of its action on the surface of a single crystal parallel to the calculated direction of $\boldsymbol{\xi}_3$ have been performed to study these states. As a result, the expected triggering of the growth of a martensite crystal has been performed [70, 80–83].

It is obvious that the dynamic structure of the initial excited state must be reproduced upon formation of a rapidly growing martensite crystal in the interphase region $B_{\gamma-\alpha}$ coinciding with the region of the front of the nonlinear transformation wave. Because the wave propagates in a metastable rather than stable medium and is far from the phase equilibrium point T_0, an increment in the energy of excitations can occur in the region of the moving front due to the energy liberated by the transforming phase. The specificity of the liberated energy conversion mechanism is important for explaining the specific features of the microscopic and macroscopic kinetics, determining the dependence of the onset temperature of the MT on the chemical composition, the effect of external fields preceding plastic deformation, and the size of grains in the polycrystal.

5. Conditions for the generation of phonons by nonequilibrium electrons

It is obvious that the region $B_{\gamma-\alpha}$ is strongly nonequilibrium. In the case of metallic systems, which are of interest for us, the extent of nonequilibrium should be characterized, along with the temperature gradient ∇T, by the gradient of the chemical potential of electrons $\nabla\mu$ (the notation μ that was used above for the shear modulus is used below for the chemical potential). The spatial scale l (Fig. 6) that specifies the width of the region $B_{\gamma-\alpha}$ in the direction $\mathbf{v}$ orthogonal to $\boldsymbol{\xi}_3$ can naturally be considered close to the transverse dimensions $d_{1,2}$ (of the order of the thickness of the plate crystal), i.e., $l \sim 0.1-1$ μm. Then the order of ∇T and $\nabla\mu$ is determined by the relations

$$\nabla T \sim \frac{\Delta T}{l} \approx \frac{T_\alpha - T_\gamma}{l} , \quad \nabla\mu \sim \frac{\Delta\mu}{l} \approx \frac{\mu_\alpha - \mu_\gamma}{l} . \tag{14}$$

The magnitude of ΔT is comparable to the degree of overcooling $T_0 - M_s$, i.e., $\Delta T \sim 100$ K, and therefore $\nabla T \sim 10^8 - 10^{10}$ K m^{-1}. The magnitude of $\Delta\mu$ can be estimated taking into account that the specific volume of the α phase increases because of the volume effect of the transformation, whereas the electron concentration n and, consequently, the chemical potential μ decrease. Assuming that $\mu \sim n^{2/3}$ (which is a standard relation between μ and n in the model of free electrons; see, e.g., [84]), we find

$$\frac{\Delta\mu}{\mu} = -\frac{2\Delta V}{3V} . \tag{15}$$

At $\Delta V/V = 2.4 \times 10^{-2}$ (the typical value for the volume change under Bain deformation) and $\mu \sim 10$ eV, we obtain $\Delta\mu = 0.16$ eV from Eqn (9), which is equivalent to 1860 K, and therefore, at the same l, the value of $\nabla\mu/k_B$ (where k_B is the Boltzmann constant) can exceed ∇T by an order of magnitude. We note that the estimation of $\Delta\mu$ based on the volume effect is valid (in view of the relation $\mu \sim n^{2/3}$) for the subsystem of s electrons. It is obvious that the same values can also be obtained for the subsystem of d electrons [19, 20].

The relatively large values of ∇T and $\nabla\mu$ necessitate the analysis of the electron and phonon subsystems of the region $B_{\gamma-\alpha}$ under nonequilibrium conditions. Such a concretization of the nonequilibrium conditions allows formulating the

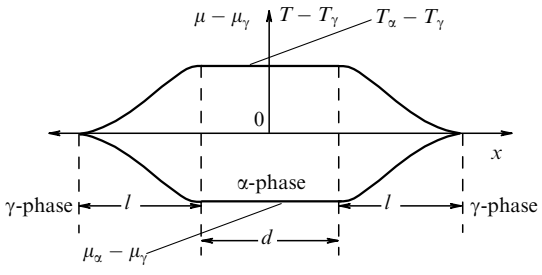

Figure 6. Tentative distribution of the temperature T and chemical potential of electrons μ upon the formation of the initial excited state. The x axis is perpendicular to the longer axis of the excited region.

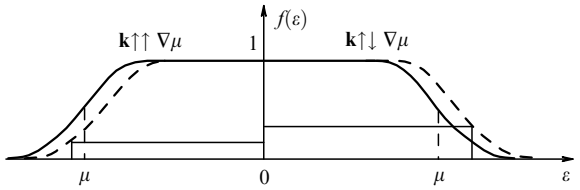

Figure 7. Equilibrium (solid lines) and nonequilibrium (dashed lines) distribution functions of electrons at $\nabla\mu \neq 0$.

question of generation (or selective amplification) of phonons by nonequilibrium electrons.

We recall that the physical basis of the maser effect is the predominance of stimulated radiation over the absorption under conditions of the inverse population of states of the radiating system (the higher the population of the states is, the higher their energy). By choosing itinerant electrons as the emitting system and assuming that the band description is valid, we can easily show that inversely populated states always exist in the presence of electron fluxes. Let $f_{j\mathbf{k}}$ be the nonequilibrium electron distribution function in the state $(j\,\mathbf{k})$, where j labels the band and $\hbar\mathbf{k}$ is the quasimomentum of an electron with an energy $\varepsilon_{j\mathbf{k}}$. With the main source of nonequilibrium $\nabla\mu \neq 0$, it is sufficient to invoke the electron distribution picture well known from the theory of electric conductivity (see, e.g., [84]) (Fig. 7).

The horizontal thin lines show the levels of populations of two inversely populated states above the Fermi level. It is obvious that there is a unidirectional movement of electrons toward a lower value of the chemical potential, i.e., against the $\nabla\mu$, and that the sign of the nonequilibrium addition to f^0 is independent of the relation between $\varepsilon_{j\mathbf{k}}$ and μ: $\Delta f_{\mathbf{k}} > 0$ for $\mathbf{k}\uparrow\downarrow\nabla\mu$ and $\Delta f_{\mathbf{k}} < 0$ for $\mathbf{k}\uparrow\uparrow\nabla\mu$. This treatment of the inversely populated states applied to nonequilibrium conditions at the stage of growth of the α phase was suggested in [85–87].

We recall the conditions necessary for the excitation (or amplification) of a plane wave of atomic displacements by nonequilibrium electrons in the case of a crystal with homogeneous and stationary gradients of the chemical potential. From the quantum standpoint, the wave of displacements $u(\mathbf{r}, t) = u_0 \cos(\omega_{\mathbf{q}} t - \mathbf{qr})$ represents a macroscopic ensemble of coherent phonons with energies $\hbar\omega_{\mathbf{q}}$ and wave vectors $\mathbf{q}$. The maser mechanism of generation of a wave is possible if there is a macroscopic number R of pairs $(\mathbf{k}, \mathbf{k}')$ of inversely populated electron states (IPESs) such that, upon transitions between them, a preferred emission of phonons occurs and the laws of energy and quasimomentum conservation are satisfied:

$$\varepsilon_{j\mathbf{k}} - \varepsilon_{j'\mathbf{k}'} = \hbar\omega_{i\mathbf{q}}\,, \quad \hbar\mathbf{k} - \hbar\mathbf{k}' - \hbar\mathbf{q} = 0,\ \hbar\mathbf{Q}\,. \tag{16}$$

Here, i labels the phonon branch and the equality to zero or to the reciprocal-lattice vector $\mathbf{Q}$ is determined by whether the electron transitions refer to normal (N) processes or to the Unclamp (U) processes [84] (Fig. 8). Thus, the problem arises of searching (in k space) for macroscopic sets of pairs of equispaced IPESs [equispaced in the sense of relations (16)].

By analogy with the case of the photon maser [88], it can easily be shown [19, 20, 89, 90] that the following threshold condition is sufficient for the realization of a phonon maser:

$$\sigma_0 > \sigma_{\text{th}}\,, \quad \sigma_{\text{th}} = \frac{\hbar^2 \Gamma \varkappa}{W^2 R_{\text{eff}}}\,, \tag{17}$$

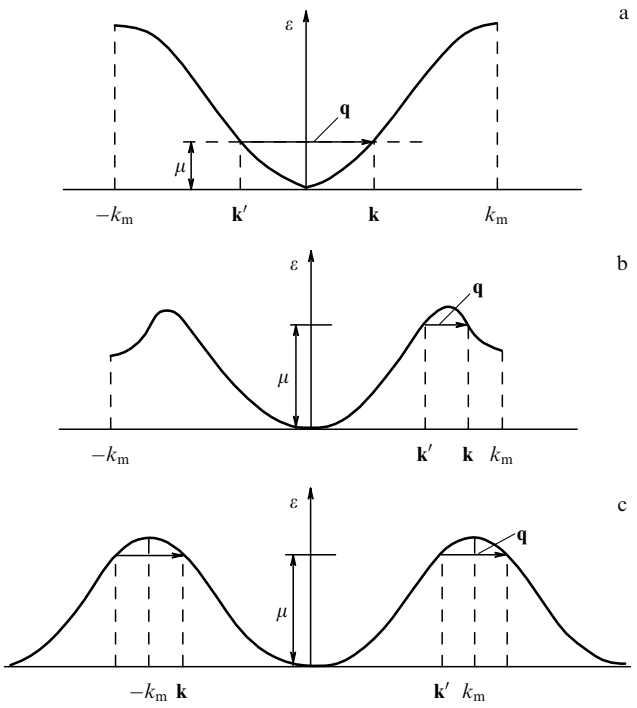

Figure 8. One-dimensional scheme of (a, b) normal processes (N processes) and (c) Umclapp processes (U processes); k_{m} is the boundary momentum of the first Brillouin zone; $\mathbf{q}$ is the momentum of the phonon; the difference between the energies $\varepsilon_{\mathbf{k}}$ and $\varepsilon_{\mathbf{k}'}$ is not taken into account; μ is the Fermi level.

where σ_0 is the initial inverse population, which is proportional to $\nabla\mu$, σ_{th} is the threshold value of the difference of the inverse populations, Γ and $\varkappa$ are respectively the electron attenuation and phonon attenuation (measured in [rad s^{-1}]), W is the matrix element of the electron–phonon interaction, and R_{eff} is the number of IPES pairs in the accessible range of energies Δ near μ. Realistic estimates of the parameters in [19, 20, 89, 90] show that condition (17) can always be satisfied in iron alloys with $\Delta \approx 0.2$ eV if the area ΔS_{eff} of the surface S separating pairs of IPESs in the k space is large (compared with the area of the first Brillouin zone) [76, 91]. In [19, 20, 92–96], the existence of large S surfaces was demonstrated using the example of electron spectra in the tight-binding approximation both for ideal fcc and bcc lattices and for the action of uniaxial and plane deformation exceeding the threshold deformation by an order of magnitude. In particular, in the case of a compressive deformation ε_2 of the initial fcc lattice along $[001]_\gamma$ with the interaction of only nearest neighbors taken into account, we obtain the spectrum

$$E(k) = E_0 - 4E_1\left[\cos\eta_1\cos\eta_2 + \frac{2}{1+(1+\varepsilon_2)^2}\cos\eta_3(1+\varepsilon_2)(\cos\eta_1+\cos\eta_2)\right]. \tag{18}$$

The use of such spectra immediately yields an analytic form of the field of group velocities $\mathbf{v}_{\mathbf{k}}$ necessary to determine the S surface that ensures the vanishing of the projection of the group velocity $\mathbf{v}_{\mathbf{k}}$ of electrons onto the direction of $\nabla\mu$:

$$\mathbf{v}_{\mathbf{k}}\nabla\mu = 0\,. \tag{19}$$

In this case, in the space of quasimomenta, the IPES pairs that have different signs of the nonequilibrium additions to f^0

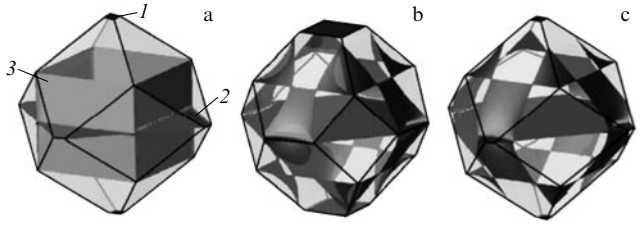

Figure 9. *S* surfaces for a uniaxially compressed initial fcc lattice: (a) taking only nearest neighbors into account at $\varepsilon_2 = -0.25$ (*1*, *2*, *3* are the planar sheets of the *S* surface); (b) taking the nearest and next-to-nearest neighbors into account at $\varepsilon_2 = -0.08$; and (c) taking the nearest and next-to-nearest neighbors into account at $\varepsilon_2 = -0.25$.

(proportional to $\mathbf{v_k}\nabla\mu$) in the presence of electron fluxes are located on opposite sides of the *S* surface. For illustration, in Fig. 9 (taken from [96]), the *S* surfaces are shown in the case where $\nabla\mu \,||\, [001]_\gamma$ (spectrum (18) corresponds to the case shown in Fig. 9a). In addition, these spectra exhibit a single peak in the density of states. Therefore, by determining the energy of the peak ε_t, we can choose the position of the level of μ corresponding to the inequality

$$|\varepsilon_d - \mu| \approx |\varepsilon_t - \mu| \leqslant \Delta\,, \tag{20}$$

where ε_d is the energy of d electrons that have energies in the region adjacent to the energy ε_t of the peak in the density of states in an accessible energy interval Δ in the vicinity of the Fermi level. In the presence of large segments of the *S* surface, the magnitude of σ_{th} is of the order of 10^{-3}; therefore, generation is possible for $\sigma_0 > 10^{-3}$.

We emphasize that the overwhelming number of points of the given sheets of the *S* surfaces lie inside the Brillouin zone rather than on its faces. Therefore, elementary acts of emission of phonons with small wave vectors ($q \ll \pi/a$) that are caused by $\mathbf{k} \to \mathbf{k}'$ electron transitions localized near the *S* surfaces are normal processes. This means that under the nonequilibrium conditions of the $\gamma \to \alpha$ martensitic transformation, just the longitudinal (quasilongitudinal) waves are mainly generated or become amplified. Indeed (see, e.g., [84, 97]), for purely transverse waves with polarization vectors $\mathbf{e_q}$ in the case of normal processes, the scalar product $\mathbf{e_q}\,\mathbf{q}$ and, consequently, the matrix element of the electron–phonon interaction *W*, which is proportional to $\mathbf{e_q}\,\mathbf{q}$, vanish. Hence, just the longitudinal waves generated by the initial excited state are mainly supported by the nonequilibrium electron subsystem.

6. Relation between the spatial scales that is characteristic of the process of heterogeneous nucleation

We now estimate the distance *r* from the dislocation line to the site of the localization of the initial excited state and the magnitude μ of its transverse size (see Figs 4 and 10). The elastic field of the defect is approximately homogeneous over the section of the parallelepiped (on a scale of the order of *d*) if the condition

$$\frac{d}{r} \leqslant 0.1 \tag{21}$$

is satisfied. Let a rectilinear segment of a separate dislocation play the role of a nucleation center and the average spacing between the dislocations be equal to *L*. Then the effect of

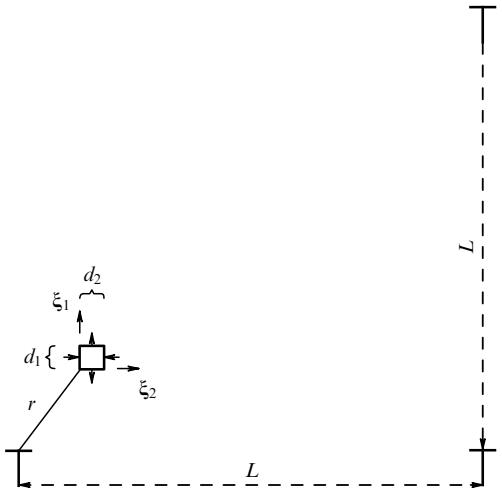

Figure 10. Region of localization of the initial excited state in the elastic field of a separate dislocation (relation between the scales *L*, *r*, and *d*).

other dislocations can be neglected if

$$r \sim 0.1L\,. \tag{22}$$

But the spacing *L* is related to the density of dislocations ρ as

$$L \sim \frac{1}{\sqrt{\rho}}\,. \tag{23}$$

It is clear from (21)–(23) that

$$d \sim 10^{-2}L \sim 10^{-2}\rho^{-1/2}\,. \tag{24}$$

It is natural to assume the dislocation density $\rho \sim 10^4$ cm^{-2}, typical of annealed single crystals as the lower boundary of ρ. From (24), we then obtain $d \sim 1$ μm. We recall that the sizes $d_{1,2}$, which are of the order of half-wavelengths that control the growth of a martensite crystal, specify the thickness of platelike martensite crystals (or the thickness of the midrib). Such thicknesses are characteristic of the first coarse crystals of martensite that appear in single-crystal samples or in coarse grains of polycrystals (with the diameter about 100 μm). We emphasize that condition (21) of the approximate homogeneity of elastic deformation over the transverse section of a nucleus can formally be satisfied by taking even smaller values of *d* (naturally, the choice of *d* smaller than the lattice parameter *a* makes no physical sense). But we deliberately use the maximum values of *d* that are still consistent with requirement (21) for our estimation: during a first-order transition, the higher the liberated energy is, the smaller the ratio of the area of the nucleus surface S_N to the nucleus volume V_N. For the nucleus that is of interest for us, i.e., in the form of a rectangular parallelepiped with the edge lengths d_1, d_2, and *l*, we obtain

$$\frac{S_N}{V_N} = 2\left(\frac{1}{d_1} + \frac{1}{d_2} + \frac{1}{l}\right), \tag{25}$$

and hence an increase in the nucleus size (in particular, in its transverse size) promotes an increase in the corresponding liberated energy.

It is clear that choosing *d* to be equal to the maximum value d_m that is still consistent with requirement (21) does not

contradict the condition of smallness of the threshold deformations $\varepsilon_{1,2\,\mathrm{th}}$:

$$\varepsilon_{1\mathrm{th}},\ |\varepsilon_{2\mathrm{th}}| < \varepsilon_{\mathrm{el}} \sim (10^{-4}-10^{-3}) \ll 1\,, \tag{26}$$

because the elastic deformation $\varepsilon_{\mathrm{ed}}$ created by a rectilinear dislocation is proportional to $1/r$ and an increase in d_{m} under condition (21) presumes an increase in r as well. Naturally, $L(\rho)$, $r(\rho)$, and $d(\rho)$ decrease with increasing the dislocation density. We note that the value of the macroscopic elastic limit given in (26) is in fact determined by the threshold condition for the generation of dislocations in single crystals or in coarse-grain polycrystals. With decreasing characteristic spatial scales, for example, under the transition to the range $\leqslant 100$ nm typical of the nanocrystalline state and of the periods of the structures of transformation twins, the elastic limit must increase, remaining less than the yield stress. Because a standard dislocation source inside a grain with diameter D can, according to [98], switch on at critical stresses $\tau_{\mathrm{c}}(D) > 3Gb/D$, where G is the shear modulus and b is the Burgers vector, the value $3b/D$ specifies the order of deformation corresponding to the yield strength (for sources at the grain boundary, $\tau_{\mathrm{c}}(D)$ is lower by a factor of 1.5). This means that the elasticity limit $\varepsilon_{\mathrm{el}}(D)$ in a grain with a characteristic size D is limited by the value $\tau_{\mathrm{c}}(D)/G = 3b/D \approx 3a/D$. At $D \sim 100$ nm and $a \sim 0.35$ nm, we have $\varepsilon_{\mathrm{el}}(D) \leqslant 10^{-2}$. Consequently, in the nanorange, at $100 > D > 10$ nm, introducing the notation $\varepsilon_{\mathrm{el}}(D) = \varepsilon_{\mathrm{el}}^{\mathrm{nano}}$, we obtain $10^{-2} \leqslant \varepsilon_{\mathrm{el}}^{\mathrm{nano}} < 10^{-1}$, where the upper limit approaches the theoretical yield strength.

Thus, the transverse size d of thin-plate crystals is specified by the magnitude of the defect-free volume of size L, which, according to (24), is of the order of magnitude of one-hundredth of L. At the beginning of the transformation in single crystals or in coarse grains, the scale L can be roughly estimated through the average dislocation density. Naturally, there is no strictly periodic dislocation lattice, and in reality the first crystals with the greatest thickness appear in regions with the greatest values of $L_{\max}$. In passing to fine crystals, the role of L is played by the grain diameter D. If the grain contains a single dislocation, then, refining relation (24) according to [99], we can assume that

$$d \approx n^{-1}10^{-2}D\,. \tag{27}$$

In (27), the lower boundary of n ($n = 1$) refers to the case where a rectilinear segment of a dislocation line lies near a planar region of a grain boundary (in the limit case, there is a grain-boundary step). Then the distance L (to the opposite boundary of the grain) is equal to D. If the dislocation line is located in the center of the grain, then L is not greater than $D/2$, and $n = 2$. This means that the values of n from the range $1 < n < 2$ correspond to an intermediate position of a single dislocation in the grain.

After the appearance of martensite crystals, additional parameters appear (and become determining); these are the dimensions L of the volumes of preserved austenite, which are either completely framed by martensite crystals or include grain-boundary fragments. It is clear that each new generation of crystals leads to a decrease in the value of L necessary for the formation of next-generation crystals. Formally, the minimum accessible L consistent with wave growth is obtained by taking d equal to the lattice parameter a. From (24) with $d_{\min} = a$, we then obtain $L_{\min} = 10^2 a$ (for example, at $a = 0.35$ nm, we have $L_{\min} = 35$ nm). For iron-based alloys, under the $\gamma-\alpha$ MT, the observed minimum (critical) grain size $D_{\min}$ depends on the chemical composition and typically exceeds $L_{\min}$ by an order of magnitude. The discussion of the critical grain size is continued in Section 8. Here, we only note that the relation between spatial scales (24) agrees qualitatively with the concept according to which the size of the newly formed inhomogeneities must be determined by the spatial scale specified by the existing system of shears (defects) [100]. However, equiaxed inhomogeneities were considered in [100], whereas the specificity of MTs dictates the formation of the initial excited states in the form of elongated parallelepipeds.

7. Region of a concerted variation of temperature and attenuation of s electrons that is optimum for the realization of the martensitic transformation

In the approximation of the relaxation time τ (see, e.g., [84, 101]), we restrict ourselves to the consideration of stationary nonequilibrium additives to $f_{\mathbf{k}}^0$ that are related to the gradient of the chemical potential as

$$f_{\mathbf{k}} - f_{\mathbf{k}}^0 \approx \frac{\partial f_{\mathbf{k}}^0}{\partial y_{\mathbf{k}}}\,\frac{\tau}{k_{\mathrm{B}}T}\,\mathbf{v}_{\mathbf{k}}\nabla\mu\,, \tag{28}$$

$$f_{\mathbf{k}}^0 = \frac{1}{\exp(y_{\mathbf{k}})+1}\,,\quad y_{\mathbf{k}} = \frac{\varepsilon_{\mathbf{k}}-\mu}{k_{\mathrm{B}}T}\,, \tag{29}$$

where $\varepsilon_{\mathbf{k}}$ is the energy of an electron with a quasimomentum $\mathbf{k}$. Assuming for simplicity that $\mathbf{v}_{\mathbf{k}} \approx -\mathbf{v}_{\mathbf{k}'}$, we represent σ_0 as

$$\sigma_0(\nabla\mu) = f_{\mathbf{k}} - f_{\mathbf{k}'} \approx \frac{\partial f_{\mathbf{k}}^0}{\partial y_{\mathbf{k}}}\,\frac{2\tau}{k_{\mathrm{B}}T}\,\mathbf{v}_{\mathbf{k}}\nabla\mu\,. \tag{30}$$

That the condition $\sigma_0 > \sigma_{\mathrm{th}}$ is satisfied in a wide range of concentrations C_{Le} of alloying elements can be substantiated in terms of a two-band model, assuming that the attenuation Γ_{s} of mobile s electrons is comparable to the quantity $(\varepsilon_{\mathrm{d}}-\mu)\,\hbar^{-1}$ and is many times greater than the attenuation Γ_{d} of 3d electrons that are active in the generation of phonons (the lifetime $\tau_{\mathrm{s}} \sim 10^{-15}$ typical of 3d metals corresponds to $\hbar\Gamma_{\mathrm{s}} \sim 0.6$ eV). Indeed, the population of states with energies $\varepsilon_{\mathrm{d}} > \mu$ can be maintained at a sufficiently high level $f_{\mathrm{d}}^0 \sim 0.1$ due to the scattering of s electrons with energies ε_{s} from the range

$$\mu - \frac{\hbar\Gamma_{\mathrm{s}}}{2} < \varepsilon_{\mathrm{s}} < \mu + \frac{\hbar\Gamma_{\mathrm{s}}}{2} \tag{31}$$

into d states.

In the presence of s–d scattering, the thermal excitation level $k_{\mathrm{B}}T$ can be much less than $\varepsilon_{\mathrm{d}} - \mu$ without a decrease in the population of d states. Similarly, for states with $\varepsilon_{\mathrm{d}} < \mu$ at $\mu - \varepsilon_{\mathrm{d}} > k_{\mathrm{B}}T$, the mechanism of d–s scattering leads to an additional smearing of the distribution of d electrons. As a result, $\hbar\Gamma_{\mathrm{s}}$ plays a role similar to that of $k_{\mathrm{B}}T$ and the d electrons are distributed in the energy range $\mu-\hbar\Gamma_{\mathrm{s}}/2-k_{\mathrm{B}}T < \varepsilon_{\mathrm{d}} < \mu+\hbar\Gamma_{\mathrm{s}}/2+k_{\mathrm{B}}T$. If $\varepsilon_{\mathrm{t}} > \mu$ and $\varepsilon_{\mathrm{t}} \in (\mu,\ \mu+\Delta)$, the following condition should be satisfied for the d states to be populated at $k_{\mathrm{B}}T \ll \hbar\Gamma_{\mathrm{s}}$:

$$\frac{\hbar\Gamma_{\mathrm{s}}}{2} \approx \bar{\varepsilon}_{\mathrm{d}} - \mu\,, \tag{32}$$

where $\bar{\varepsilon}_d$ plays the role of the mean energy of the above interval. The attenuation Γ_s can naturally be represented as the sum

$$\Gamma_s(T, C, d) = \Gamma_s(T) + \Gamma_s(C) + \Gamma_s(d) . \quad (33)$$

In (33), the term $\Gamma_s(T)$, related to the scattering on thermally activated inhomogeneities (vacancies, phonons, magnons, and so on) decreases with decreasing T; in the case of a binary alloy, the attenuation $\Gamma_s(C) \sim C(1 - C)$ is related to impurity scattering (C is the concentration of the alloying additive); the term $\Gamma_s(d)$, according to [102], is due to the effect exerted by s electrons on the attenuation due to inhomogeneity with a characteristic transverse spatial scale d that is due to the liberation of energy in the region where the excited state arises (i.e., $d \approx d_{1,2}$); earlier [19, 20, 103], this effect was ignored. If the crystals do not have the internal twin structure, then d is a characteristic mesoscopic scale of the active region in which the wave beam generation process occurs. Upon the formation of twinned crystals, when short-wavelength displacements are also included in the control wave process, the d_{tw} scale of the order of the thickness of the twin main component ($d_{tw} \ll d$) should also be taken into account.

We estimate $\Gamma_s(d)$. We recall that the characteristic time τ_s necessary for s electrons to intersect a region of size d is

$$\tau_s \approx \frac{d}{v_s} . \quad (34)$$

According to the uncertainty relation for energy and time, we then have

$$\hbar\Gamma_s(d) \approx \frac{\hbar}{2\tau_s} \approx \frac{\hbar v_s}{2d} . \quad (35)$$

With the relation between the scales given in (27), formula (35) can be rewritten in the form explicitly containing the grain size:

$$\hbar\Gamma_s(d) \equiv \hbar\Gamma_s(D) \approx 10^2 n \frac{\hbar v_s}{2D} . \quad (36)$$

It is obvious from (36) that in the case of small d, the contribution $\Gamma_s(D)$ becomes comparable to the contributions $\Gamma_s(C)$ and $\Gamma_s(T)$, whereas for single-crystal samples and coarse grains, this contribution can be neglected. We assume that D is large and that the change in $\bar{\varepsilon}_d - \mu$ related to the change in C can be ignored. Then (32) can be satisfied in wide ranges of T and C values, because an increase in $\Gamma_s(C)$ upon a decrease in $\Gamma_s(T)$ smooths the function $\Gamma_s(C, T)$, stabilizing the degree of smearing of the distribution of d electrons. Consequently, it is necessary to modify the form of the equilibrium distribution function $f^0 \Rightarrow \tilde{f}^0$ such that $\tilde{f}^0$ can account for the smearing of the distribution caused by changes in T and Γ_s, and then investigate the behavior of the derivatives $\partial\tilde{f}_0/\partial\mu$, which determine, along with the values of the gradient $\nabla\mu$, the magnitude of the difference of populations σ_0. In essence, it is necessary to find the ranges of T and Γ_s in which σ_0 reaches a maximum at a fixed $|\bar{\varepsilon}_d - \mu|$. It is natural to assume that the temperature T in this region is the temperature $\widetilde{T}$ optimum for the occurrence of the MT. Requiring that the $\widetilde{T}(C)$ and $M_s(C)$ dependences be similar and choosing the electron configuration of one of the alloy components as the reference one, we can find the electron configuration of the other component. Such a formulation of the problem was used in [19, 20, 103] for substitutional (Fe–Ni, Fe–Mn) and interstitial (Fe–C) alloys.

The modified distribution function $\tilde{f}^0$ is given by

$$\tilde{f}^0_{\mathbf{k}} = \int_{-\infty}^{\infty} \left[1 + \exp\left(\frac{\varepsilon - \mu}{k_B T}\right)\right]^{-1} A(\varepsilon, \mathbf{k})\, d\varepsilon , \quad (37)$$

where the spectral density $A(\varepsilon, \mathbf{k})$ is the probability, averaged over the configurations, of finding an electron with an energy ε and a quasimomentum $\hbar\mathbf{k}$ in the alloy. Usually, the spectral density has a Lorentzian shape:

$$A(\varepsilon, \mathbf{k}) = \frac{1}{\pi} \frac{1/2\hbar\Gamma_{\mathbf{k}}}{(\varepsilon - \varepsilon_{\mathbf{k}})^2 + (1/2\hbar\Gamma_{\mathbf{k}})^2} , \quad (38)$$

where $\Gamma_{\mathbf{k}}$ is the attenuation of an electron with an energy $\varepsilon_{\mathbf{k}}$. As $\Gamma_{\mathbf{k}} \to 0$, the function $A(\varepsilon, \mathbf{k})$ transforms into a δ function, and function (37) transforms into the function $f^0_{\mathbf{k}}$ given by (29). We introduce the dimensionless chemical potential $\mu' = \mu/|\bar{\varepsilon}_d - \mu|$ and the variables

$$\Gamma' = \frac{\hbar\Gamma}{2|\bar{\varepsilon}_d - \mu|} , \quad T' = \frac{k_B T}{|\bar{\varepsilon}_d - \mu|} . \quad (39)$$

Assuming that in the case of $\varepsilon_{\mathbf{k}} = \varepsilon_{\mathbf{kd}}$, in view of a strong s–d scattering, $\tilde{f}^0_d$ can be taken equal to f^0_s given by (37), we omit the indices d and 0 and the tilde over f^0_d in what follows. To find the optimum region of the variation of T' and Γ', for fixed values $|\bar{\varepsilon}_d - \mu|$ and $\tau\mathbf{v}\nabla\mu$, it then suffices to investigate the behavior of the derivative $\partial f/\partial\mu'$. The results of the calculations of $\partial f/\partial\mu'$ are given in Fig. 11.

The families of thin lines are isolines, on which the derivative $\partial f/\partial\mu'$ takes constant values (indicated in the figure), and dashed lines *1* and *2* are respectively determined by the conditions

$$\frac{\partial}{\partial T'}\left(\frac{\partial f}{\partial\mu'}\right)\Big|_{\Gamma'} = 0 , \quad \frac{\partial}{\partial\Gamma'}\left(\frac{\partial f}{\partial\mu'}\right)\Big|_{T'} = 0 . \quad (40)$$

Lines *1* and *2* correspond to maxima of the derivative $\partial f/\partial\mu'$ with respect to the variables T' and Γ' and pass through the points at which the straight lines respectively parallel to the

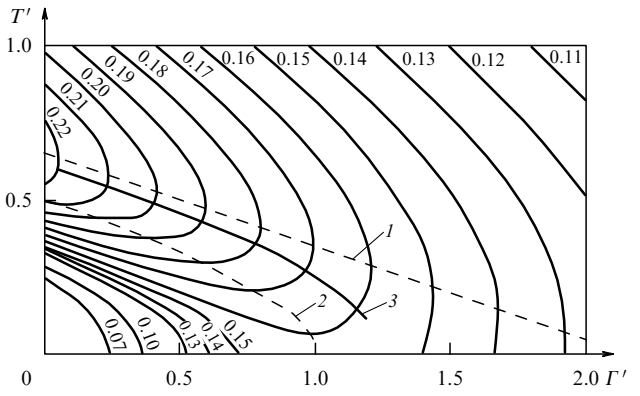

Figure 11. Results of the calculation of $\partial f/\partial\mu'$ in the case of a Lorentzian shape of the spectral density: fractional numbers correspond to the values of $\partial f/\partial\mu'$ on the family of isolines $\partial f/\partial\mu' = \text{const}$; curves *1* and *2* limit the region of a slow variation of $\partial f/\partial\mu'$ with increasing Γ' and decreasing T'.

vertical and horizontal coordinate axes touch the isolines. Solid line *3* in Fig. 11 represents a projection onto the plane (Γ', T') of the 'ridge' in the shape of $\partial f/\partial\mu'$. The regions between lines *1* and *2* correspond to the values of the parameters T and Γ at which the inverse difference of the populations $\sigma_0(\nabla\mu)$ is large. By specifying the point corresponding to pure iron inside this region, we can introduce the optimum temperature for generation of phonons, which decreases with increasing the attenuation Γ (such are the dependences $T'(\Gamma')$ for lines *1*, *2*, and *3*). Therefore, the behavior of the derivative $\partial f/\partial\mu'$ indicates the possibility of introducing an optimum temperature $\widetilde{T}$ satisfying the condition $\partial\widetilde{T}/\partial C < 0$.

As follows from experiments on rapid cooling [104–108], four values of M_s are observed in pure iron: $M_s^{\mathrm{I}} = 820\,^{\circ}\mathrm{C}$, $M_s^{\mathrm{II}} = 720\,^{\circ}\mathrm{C}$, $M_s^{\mathrm{III}} = 540\,^{\circ}\mathrm{C}$, and $M_s^{\mathrm{IV}} = 430\,^{\circ}\mathrm{C}$. Correspondingly, there are four branches of concentration dependences $M_s^i(C)$ in alloys. It has been shown in [19, 20, 103] that the correspondence of the point with coordinates $T_0' \approx 0.4$ and $\Gamma_0' \approx 0.4$ to the temperature M_s^{I} agrees with the electron configurations close to $3d^{8.6}4s^{1.4}$ for Ni atoms and to $3d^74s^1$ for Fe atoms in the case of mapping the observed concentration dependences $M_s^i(C)$ onto the region close to the vicinity of line *2* in Fig. 11. The following coordinates $(T_0', \Gamma_0')^i$ correspond to the initial points of the branches of $\widetilde{M}_s^i$:

$$\widetilde{M}_s^{\mathrm{I}} \to (0.397,\, 0.417)^{\mathrm{I}}, \quad \widetilde{M}_s^{\mathrm{II}} \to (0.361,\, 0.379)^{\mathrm{II}}, \qquad \widetilde{M}_s^{\mathrm{III}} \to (0.296,\, 0.310)^{\mathrm{III}}, \quad \widetilde{M}_s^{\mathrm{IV}} \to (0.256,\, 0.268)^{\mathrm{IV}}. \tag{41}$$

The electron attenuation was represented in the form $\Gamma(T, C) = \Gamma(T) + \Gamma(C)$; the temperature dependence was assumed to be linear,

$$\hbar\Gamma_s(T) = a_0 k_B T, \tag{42}$$

where a_0 is a dimensionless parameter and $|\bar{\varepsilon}_d - \mu| \approx 0.237$ eV. In a temperature range close to the Debye temperature T_D, a satisfactory description of $\Gamma_s(T)$ was obtained at $a_0 \approx 2.1$. By keeping the form of (42) in processing data for temperatures below room temperature, the coefficient a_0 should be considered temperature dependent, because there are several contributions to the attenuation $\Gamma_s(T)$ that are proportional to T^P with different P. In [102], we took $a_0 \approx 1$ as the maximum value of a_0 in this temperature range.

To describe the effect of the parameters C and D on the M_s temperature, it is suitable to specify the analytic approximations of the 'trajectories' that connect the initial point $\widetilde{M}_s^i$ of the ith branch with the end point for the ith concentration dependence on the plane (Γ', T'). Important conclusions can be obtained, for example, from considering the parabolic approximation [102] for curve *2* in Fig. 11 passing through the points $(\Gamma' = 1,\ T' = 0)$ and $(\Gamma' = 0,\ T' = 0.5)$:

$$1 - \Gamma' = 4T'^2. \tag{43}$$

It follows from (43) that $T' \to 0$ as $\Gamma' \to 1$. We note that for electron configurations close to $3d^{8.6}4s^{1.4}$ for Ni atoms and to $3d^74s^1$ for Fe atoms, the representation of the dependence $\widetilde{M}_s^{\mathrm{I}}(C)$ is close to (43).

8. Critical size of austenite grains in polycrystals

The discovery of a concerted variation of the parameters T' and Γ' opens the possibility of interpreting the M_s temperature as the optimum one for the occurrence of an MT and obtaining an analytic formula for the dependence of M_s not only on the concentration of an alloying element [19, 20, 103] but also on the grain size [99, 102]. This simultaneously allows solving the problem of the existence of a critical size D_c of crystallites (grains) in polycrystalline austenite such that an MT cannot even be induced at $D \leqslant D_c$ by cooling to absolute zero, in other words, the condition

$$M_s(D_c) = 0 \tag{44}$$

is satisfied. We recall that the existence of a critical size D_c was revealed as long ago as 1929 [109]; in [110], a strong dependence of D_c on the alloy composition demonstrated. Nevertheless, in spite of numerous studies devoted to this problem (e.g., [111–119]), no consistent treatment of the discovered regularities could be obtained (the main difficulties are discussed in detail in [99]).

After substituting attenuation (33) in (43) and using (42), (36), and (44), we find

$$\widetilde{T}' = -\frac{a_0}{16} + \sqrt{\left(\frac{a_0}{16}\right)^2 + \bigl(1 - \Gamma'(C)\bigr)\,\frac{1 - D_c/D}{4}}, \tag{45}$$

$$D_c = \frac{\hbar n 10^2 v_s}{4|\,\bar{\varepsilon}_d - \mu|\bigl(1 - \Gamma'(C)\bigr)}. \tag{46}$$

The other solution in (45) (with the minus sign before the square root) is rejected because it leads to $\widetilde{T}' < 0$. With the true temperature dependences $\Gamma'(T)$, equations involving the temperature in powers greater than two can be obtained, which can lead to several physically realized branches of $M_s(C)$. As was noted above, up to four branches can be revealed. But the manifestation of the effect of the critical dependence of M_s on the grain size can most suitably be observed in those alloys whose M_s temperature lies in the range from room temperature to absolute zero, where only one branch, $M_s^{\mathrm{IV}}(C)$, is in fact preserved, which virtually merges with the $M_s^{\mathrm{I}}(C)$ branch.

Formula (46) reflects the change in the chemical composition of the alloy through the change in the parameter $\Gamma'(C)$; the contribution of each component depends on its electron configuration. The effect of the structure is represented in (46) directly, through the factor $n \times 10^2$, which determines the ratio of the scales D/d (or L/d) in accordance with (27).

If the temperature of the initial phase exceeds the magnetic ordering temperature T_c, then the parameter $|\,\bar{\varepsilon}_d - \mu|$ changes only weakly. In particular, for $T > T_D$ (and Ni concentrations below 27%), the value $|\,\bar{\varepsilon}_d - \mu| \approx 0.237$ eV was chosen, which was used, along with $a_0 \approx 2.1$, in mapping (41). But in the case of concentrated alloys (> 27% Ni), the temperature T_c exceeds M_s, the magnitude of $|\,\bar{\varepsilon}_d - \mu|$ corresponds to that for the spin-polarized state of electrons, and its change is of the order of 10%.

It follows from (46) that at values of $\Gamma'(C)$ approaching unity, the critical size D_c increases and becomes equal to infinity at $\Gamma'(C) = 1$; in this case, according to (45), $\widetilde{T}$ vanishes:

$$\Gamma'(C) \to 1, \quad D_c \to \infty, \quad \widetilde{T}(D) \to \widetilde{T}(D_c) \to 0. \tag{47}$$

Such a situation occurs for the Fe–Ni system (when the Ni concentration C_{Ni} approaches a certain value C^*, $33\% < C^* < 35\%$). Taking (32) into account, it is natural to assume that $\Gamma'(C^*) = 1$ is the maximum admissible value. Indeed, (32) is equivalent to the condition

$$\Gamma'(D, C, T) = \Gamma'(C) + \Gamma'(D) + \Gamma'(T) = 1 \tag{48}$$

for the complete attenuation of s electrons. It is clear that $\Gamma'(T) \to 0$ as $T \to 0$ and that $\Gamma'(D) \to 0$ as $D \to \infty$; but we then have $\Gamma'(C) \to 1$ from (48). Thus, the limit case in (47) receives a simple interpretation. The contribution $\hbar\Gamma(C)$ to the smearing of the energy of the state of s electrons is sufficient to populate states with the energies $|\bar{\varepsilon}_d - \mu|$. Therefore, no additional contributions (connected with scattering on thermally activated inhomogeneities) to the broadening of the energy levels of s electrons (important for populating d states, which can acquire nonequilibrium additives) are now required.

It is important that on the plane (T', Γ') (in the formulation of the problem under consideration), only the region

$$\Gamma' \leqslant 1 \tag{49}$$

is accessible. Constraint (49) allows understanding the reason for the existence of a strict upper concentration boundary of alloy compositions for the occurrence of the martensitic reaction: this boundary corresponds to the kinetic phase diagram of the realization of the MT controlled by the displacement waves generated at the stage of growth by nonequilibrium d electrons.

It is also obvious that formula (46) for the critical grain size is a consequence of the relation between spatial scales (27) and of the uncertainty relations for energy and time (35) and (32); i.e., it is of fundamental character.

If we neglect contribution (42) to the attenuation, we obtain the following simple formula from (45) at $a_0 = 0$:

$$\widetilde{T}(D) = \widetilde{T}_\infty \sqrt{1 - \frac{D_c}{D}},$$

$$\widetilde{T}_\infty = \widetilde{T}(\infty) = |\bar{\varepsilon}_d - \mu| \, \frac{\sqrt{1 - \Gamma'(C)}}{2k_B}. \tag{50}$$

In the case of twinned crystals, the contribution $\Gamma(d_{tw})$ to the attenuation of s electrons caused by the additional scale d_{tw} can be found similarly to (35); in this case, the substitutions $\Gamma'(C) \to \Gamma'_e$ and $\Gamma(C) \to \Gamma_e$, where $\Gamma'_e = \Gamma'(C) + \Gamma'(d_{tw})$ is the 'effective' attenuation, should be made in all the formulas. At $\Gamma'(d_{tw})$, $d_{tw} \approx 20a \approx 7 \times 10^{-9}$ m $= 7$ nm, $v_s \approx 10^6$ m s^{-1}, $|\varepsilon_d - \mu| \approx 0.237$ eV, and $\hbar \approx 1.054 \times 10^{-34}$ J s, the estimation yields $\Gamma'(d_{tw}) \approx 0.0992 \approx 0.1$. This is a significant contribution, because the maximum range (for the branch $\widetilde{M}_s^{IV}$) of the variation of Γ' (for substances from pure iron to an alloy with the concentration C^*) is limited by the inequalities $0.268 \leqslant \Gamma' \leqslant 1$.

In the general case, each system should be characterized, apart from a concrete choice of the data (T'_0, Γ'_0) for the main component of the alloy, by its own set of parameters (a_0, n, $|\bar{\varepsilon}_d - \mu|$, v_s, $\Gamma'(C)$). It can be seen from (46) that D_c is independent of the parameter a_0, but $\widetilde{T}(\infty)$ depends on a_0, as follows from (45). We recall that a_0 should be regarded as a T-dependent parameter.

A more detailed analysis [102] shows that the use of (45) and (46) can yield a detailed agreement with the experimental data in [110] for MTs in the Fe–31Ni and Fe–31Ni–0.28 C systems (with $D_c \approx 1$ and $D_c \approx 10$ μm, respectively). Therefore, it is natural to identify the $\widetilde{T}(D)$ and $M_s(D)$ dependences, i.e., to assume that $\widetilde{T} \equiv M_s$. Hence, the process of approaching the preferred concentration C^* is correctly reflected by (45) and (46) at Γ' close to unity. One more limit case also follows from (46): D_c achieves a minimum value at $\Gamma'(C) \to 0$ (i.e., in the case of pure iron) and $n = 1$. Assuming additionally that $|\bar{\varepsilon}_d - \mu| \approx 0.237$ eV $= 0.3792 \times 10^{-19}$ J and $v_s \approx 10^6$ m s^{-1}, we obtain $D_c^{min} \approx 70$ nm from (46). We note that this estimate of D_c^{min} exceeds the magnitude of L_{min} only twofold (see the end of Section 5). However, in the nanocrystalline state (e.g., at $D < 100$ nm), the CWP cannot contain long-wavelength components, and a specific realization of an accommodation MT is possible [120].

9. Dynamic model of the formation of twinned martensite crystals

Describing the process of the formation of a regular twin structure (TS) under conditions of supersonic growth of a martensite crystal is the most complex problem of the dynamic theory of MTs.

The alternating layers of the main and twinned components of the TS have orthogonally oriented (in the initial phase) principal compression axes $\langle 100 \rangle_\gamma$ and $\langle 010 \rangle_\gamma$, and the common tensile axis $\langle 001 \rangle_\gamma$. The ratio β of the volume fractions of the twin components apparently lies in the interval $1 < \beta < 2$, and the joining on planes $\{110\}_\gamma$, which pass into planes $\{112\}_\alpha$, is assumed to be almost coherent.

In [78], we formulated a hypothesis according to which the control of the TS formation should be interpreted as a consequence of concerted propagation of relatively short-wavelength and long-wavelength displacements of atoms. This means that the dynamic structure of the CWP should be developed further. We conventionally call the pairs of quasilongitudinal displacement waves (with wavelengths of the order of the thickness of a martensite plate, $\lambda_l \sim (0.1-1)$ μm), which are responsible for the formation of the habit plane, long-wavelength waves or, for short, l waves. The pairs of longitudinal waves with wavelengths $\lambda_s \sim 10^{-2}$ μm (of the order of the TS period), which propagate along the orthogonal directions $\langle 100 \rangle_\gamma$ and $\langle 010 \rangle_\gamma$ and are responsible for the formation of boundaries $\{110\}_\gamma$, are conventionally called short-wavelength or s waves.

The introduction of s waves into the structure of the CWP permitted us to develop the model of a supersonic formation of the TS, which is an important variant of the realization of a regular layered structure (RLS). The possibility of reproducing an active oscillating s cell due to the propagation of s-wave beams along the mutually orthogonal directions $[110]_\gamma$ and $[1\bar{1}0]_\gamma$ allows understanding, by taking only threshold deformations into account, how an RLS can arise in the presence of only a single initial active s cell.

The main component of the TS upon the initiation of the Bain deformation is related to the dynamic cell in the form of a rectangular parallelepiped with the edges along three orthogonal axes $\langle 001 \rangle_\gamma$. Two edges have equal sizes $d_s < \lambda_s/2$; the third size, d_{sl}, satisfies the inequalities

$$d_s \ll d_{sl} < \frac{\lambda_l}{2}.$$

The appropriateness of the choice of the dynamic cell in the form of a parallelepiped with the edges along the $\langle 001\rangle_\gamma$ axes, which is capable of initiating the emission of wave beams in these directions (and therefore the Bain deformation in the region of the formation of the main TS component) follows from experiments in [60], which showed that in the temperature range preceding the onset of the $\gamma-\alpha$ MT, only displacements along the $\langle 001\rangle_\gamma$ axes are fixed among the longitudinal oscillations with enhanced amplitudes in a wide range of wave vectors. The reason is that with the anisotropy factor of the lattice $A > 1$ in the directions $\langle 001\rangle_\gamma$, the velocities of the longitudinal sound are minimal and, consequently, the energies of the longitudinal phonons are also minimal. In addition, in alloys with compositions at which crystals are formed with habits $\{31015\}_\gamma$ (e.g., Fe–31Ni), the M_s temperature is preceded by magnetic ordering, which is accompanied, according to [50], by a decrease in the elastic modulus C_{11} by approximately 20%, which favors an additional increase in the amplitudes of oscillations in the $\langle 001\rangle_\gamma$ directions. Therefore, the conditions for the appearance of at least one necessary cell do exist, because due to the superimposition of such oscillations with a required phasing, a local fluctuation arises initiating the overcoming of the energy barrier by atoms localized in the volume of the cell. The jumps into new states at the M_s temperature are accompanied by energy liberation, which manifests itself in a sharp increase in the amplitudes of oscillations and in the emission of s-wave beams.

Upon superimposition of a pair of longitudinal s-wave beams propagating in orthogonal directions $[100]_\gamma$ and $[0\bar{1}0]_\gamma$ with velocities $\mathbf{v}_{1,2s}$ equal in magnitude, the velocity of growth of the main component of a twin $\mathbf{v}_{tw}$ in the $[1\bar{1}0]_\gamma$ direction (which is a vector sum of the velocities $\mathbf{v}_{1s}$ and $\mathbf{v}_{2s}$ according to Section 3) exceeds the velocities of the s waves by the factor $\sqrt{2}$ in the $\langle 001\rangle_\gamma$ directions:

$$v_{tw} = v_{1,2s}\sqrt{2}\,.$$

Because of the equality of the velocities, these beams, according to (13), carry deformations that are equal in magnitude but opposite in sign, $\varepsilon_{1s} = -\varepsilon_{2s}$.

The reproduction of the best conditions for the activation of a short-wavelength cell in the CWP structure can be achieved if

$$v_{1s} = v'_{2l}(\psi)\cos\psi\,, \tag{51}$$

where $v'_{2l}(\psi)$ is the projection of $\mathbf{v}_{2l}$ onto the plane $(001)_\gamma$ and ψ is the angle between the projection of the wave normal $\mathbf{n}_{2l}$ onto the plane $(001)_\gamma$ and the axis $[100]_\gamma$. Relation (51) was obtained from the equality of the times of propagation along the two legs of the right triangle in the directions $[1\bar{1}0]_\gamma$ and $[110]_\gamma$ with the velocity v_{tw} and along the hypotenuse of the triangle with the velocity $v'_{2l}(\psi)$. In Fig. 12, the hypotenuses correspond to the shortest distances connecting the centers of neighboring cells of size d_s. We note that relation (51) allows fixing the wavelength λ_s uniquely. Indeed, in calculating the velocity of l waves, we can restrict ourselves to the long-wavelength approximation (Christoffel equation), which does not fix the magnitude of λ_l, but for the shorter s waves, the value of the velocity v_s found from (51) can be uniquely assigned a λ_s using the monotonic dispersion relation for phonons along the fourfold symmetry axis.

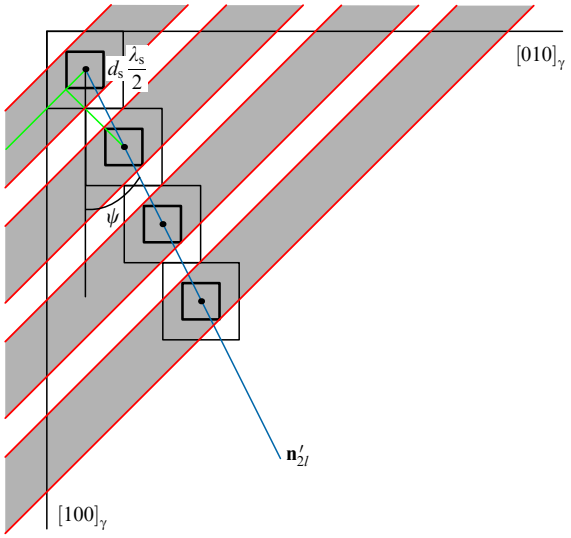

Figure 12. Dynamic model of the formation of a regular layered structure.

The emerging periodic layered structure is characterized by the ratio of the volumes of the components that depend only on the parameter d_s/λ_s and direction $\mathbf{n}_{2l}$:

$$\beta = \frac{4d_s/\lambda_s}{1+\tan\psi - 4d_s/\lambda_s}\,. \tag{52}$$

In particular, the invariant presented in Fig. 12 corresponds to the values $d_s/\lambda_s = 1/4$, $\tan\psi = 1/2$, and $\beta = 2$.

To complete the description of the MT (inter alia, of the macroshear and the mutual orientation of the lattices of the initial and final phases), it is necessary to understand the ways of passing from the threshold deformations carried by the CWP, which lie in the range of elastic deformations of the initial phase, to the final deformations, which exceed the threshold deformations by two to three orders of magnitude. We note that a fundamental solution was found in [126–130] using the example of bcc–hcp and fcc–bcc transformations in the case where the CWP stimulates the fastest rearrangement of the most close-packed planes of the initial phase without taking the twinning of the crystals into account. The key ideas are the preservation of the ratio of deformations specified by the CWP in the process of the rapid transition to final deformations and the constrained character of the deformation of the plate-like region of the lattice lacking stability. In [125], this approach was extended to the case of twinned crystals of martensite in the case of the $\gamma-\alpha$ MT and wave structure of the CWP, which stimulates the Bain deformation process. In particular, it can be easily shown that the value of the parameter $\beta = \beta_{tw}$ that is optimum for the formation of the TS corresponds to the fastest transformation of the lattice under the MT [125]. In this case, the tensile deformations ε_{1B} in the main components of the TS that border the additional component ensure the realization of the Bain deformation of compression ε_{2B} in the additional TS component. In the final result,

$$\beta = \beta_{tw} = \frac{|\varepsilon_{2B}|}{\varepsilon_{1B}}\,. \tag{53}$$

Table 1 contains summary information on the morphological features. The results of the calculations given in the

Table 1. Summary information on the morphological signs of twinned $\{3\,10\,15\}_\gamma$ crystals.

Characteristics	Experiment		Theoretical analysis		
	G–T [4]	D–B [131]	W–L–R [10]	B–M [13]	K–Ch [125]
Habit plane (HP)	0.5472 0.1642 0.8208	0.5481 0.1748 0.8180	0.5691 0.1783 0.8027	0.55102 0.18726 0.81321	0.533462 0.14318 0.833617
Angle between $(HP)_t$ and $(HP)_{G–T}$			$\approx 1.728°$	$\approx 1.284°$	$\approx 1.509°$
Orientation relations					
$(111)_\gamma^\wedge (101)_\alpha$	$\approx 1°$	$\approx 1°$	$\approx 0.25°$	$\approx 0.2°$	$\approx 1.3108°$
$[1\bar{1}0]_\gamma^\wedge [11\bar{1}]_\alpha$	$\approx 2.5°$	$\approx 2.5°$	$\approx 3°$	$\approx 2.7°$	$\approx 2.4319°$
$[\bar{2}11]_\gamma^\wedge [10\bar{1}]_\alpha$	$\approx 2°$		$\approx 1.72°$	$\approx 1.9°$	$\approx 2.3089°$
$[\bar{1}01]_\gamma^\wedge [\bar{1}11]_\alpha$	$\approx 6.5°$		$\approx 6.32°$	$\approx 6.6°$	$\approx 6.9810°$
Macroshear angle	10.66°	**10.69°**	10.33° 10.71°	**10.5395°**	10.7839°
Macroshear direction	−0.7315 −0.3828 0.5642	**−0.7914** **−0.2083** **0.5747**	−0.7660 −0.2400 0.5964	**−0.769969** **−0.261645** **0.581970**	−0.791386 −0.263371 0.551673
$\Delta\mathbf{S} \wedge \Delta\mathbf{S}_{G–T}$			$\approx 8.6°$	$\approx$ **7.3702°**	$\approx 7.7050°$
$\Delta\mathbf{S} \wedge \Delta\mathbf{S}_{D–B}$			$\approx$ **2.6081°**	$\approx$ **4.2575°**	$\approx 3.4243°$

last column were obtained for the following values of the elastic moduli (in TPa): $C_L = 0.2180$, $C' = 0.0270$, and $C_{44}^0 = 0.1120$. These moduli correspond, according to [50], to the Fe–31.5% Ni alloy at the temperature $M_s = 239$ K. Because the experimental data refer to the alloy with the composition Fe–22Ni–0.8C, the moduli used in the calculations play the role of a model set. Based on the results of the calculation of the elastic field of a dislocation loop, the following directions of the wave normals have been chosen:

$$\mathbf{n}_{1l} = [0.147188 \quad -0.987456 \quad 0.57158]_\gamma\,,$$

$$\mathbf{n}_{2l} = [0.948816 \quad 0.157282 \quad 0.273879]_\gamma\,. \tag{54}$$

Using the Christoffel equations [79] for the normals in (54), we obtain the ratio of the velocity magnitudes $\varkappa_l = v_2/v_1 \approx 1.08861$ at which the orientation of the normal to the expected habit

$$\mathbf{N}_{wl} \| [0.533462 \quad 0.14318 \quad 0.833617]_\gamma \tag{55}$$

deviates from $[10\ 3\ 15]_\gamma$ by 1.509°.

For the alloy Fe–22Ni–0.8C, according to [4], the relative change in volume under the $\gamma-\alpha$ MT is $\delta = 0.0384$ and the tetragonality of the martensite is $t = 1.045$. Then the principal Bain deformations are

$$\varepsilon_{1,3B} \approx 0.12011\,, \quad \varepsilon_{2B} \approx -0.17232\,. \tag{56}$$

In correspondence with (53) and (56), the ratio of the TS components is $\beta = \beta_{tw} \approx 1.434685$, and the fraction of the twin component is

$$\delta_{tw} = (\beta_{tw} + 1)^{-1} = \delta_{tw} \approx 0.41073\,. \tag{57}$$

Because the normals in (54) deviate from the fourfold symmetry axes, the difference between the quasilongitudinal and purely longitudinal waves noticeably affects the orientation of the eigenvectors of the deformation tensor corresponding to the l waves and therefore the results of the calculation of the orientation relations and macroshear [125].

In bold script in Table 1, we give the results of our recalculation of the data on the macroshears obtained in [13] (direction $d = [-0.21017 \quad -0.61850 \quad 0.75715]_\gamma$, magnitude of the macroshear 0.19144) and in [131] (direction $d = [-0.1761 \quad -0.6886 \quad 0.7034]_\gamma$, magnitude 0.1915) into the components of the macroshear along the habit plane. The analysis, along with the results in [4], of later experimental data [131] obtained on the same Fe–22Ni–0.8C alloy demonstrates that the macroshear direction in [131] is substantially closer to the calculated data than are those obtained in [4]. This concerns the results of calculations performed in [13, 10] and in [125].

The calculation of the morphological signs demonstrates the efficiency of the dynamic theory in the description of all the essential observed features of the $\gamma-\alpha$ reconstructive MT in iron-based alloys with a grain size exceeding the critical size D_c. Although we did not discuss the effect of the magnetic field [7, 132] on the occurrence of the MT here, we recall that the orientational effect was predicted in [76] (based on the concept of the CWP [19, 20] and analysis of nonequilibrium additives to the distribution of d electrons under a strong magnetic field) and was confirmed experimentally in [133]. In addition, it can be easily understood [134] that the magnetic field can change the parameter $|\bar{\varepsilon}_d - \mu|$. According to (46), the critical size D_c then also changes. This manifests itself most clearly in alloys with concentrations C close to the special concentration C^*, where, in the absence of a magnetic field, $\Gamma'(C) \to 1$ according to (47). Taking the variation of D_c in a magnetic field into account allows naturally explaining the observed effects of the destabilization of austenite preliminarily stabilized via grain refinement or severe plastic deformation [7].

10. Summary remarks

The limit variant of the fastest formation of a martensite crystal corresponds to the formation of an initial excited state in the elastic field of a separate dislocation, which initiates the regime of supersonic growth. The most vivid picture of an MT can be realized for transition metals and alloys when conditions of generation (amplification) of elastic waves by nonequilibrium electrons are satisfied. In this case, the long axes of the crystals are due to the process of growth whose termination is limited by the scattering of the CWP by obstacles such as boundaries of the sample, grains, and previously formed crystals. The macrokinetics can have a 'burst' autocatalytic character, because the appearance of crystals leads to the multiplication of nucleation centers [135] and the formation of certain ensembles of martensite crystals (in particular, zigzag-like; see Fig. 3). The relation between spatial scales (24) allows specifying the similarity coefficient upon the formation of sequential generations of crystals, permitting easily estimating the macroscopic amount of the arising martensite in terms of the symmetric model of crosswise-joining crystals [134, 136, 137]. The latest generation of crystals corresponds to the achievement of the critical size (of the order of D_c) for the free volumes of austenite. It is principally important that the calculation of the macroparameter is performed on the basis of a purely dynamic approach, without resort to thermodynamics. In turn, the knowledge of variable scales of the free volume and of the dependence of M_s on D allows explaining the reduction in M_s in the presence of previously formed crystals. The temperature M_f of the MT termination for an alloy of a given composition can then be interpreted as the M_s temperature of the formation of crystals of the last generation.

If the condition for generation is not satisfied, the emerging crystals have the form of laths whose width corresponds to the time of propagation of the CWP limited by the time of the reduction of the initial level of deformations to an underthreshold level. In iron alloys, such a shape is characteristic of crystals with habits close to $\{557\}_\gamma$, which are formed (beginning from low concentrations of the alloying element or an interstitial impurity) at relatively high M_s temperatures. The formation of specific ensembles of packet martensite [138] with compactly packed stacks of laths [73] exhibits isothermal macrokinetics [35]. But it must be recalled that the existence of gradients of temperature and chemical potential reduces the magnitude of the effective attenuation of elastic waves, thereby increasing the lifetime of the CWP in the overthreshold regime. The main feature of the isothermal macrokinetics is the existence of a temperature such that the deviation from it toward both higher and lower temperatures is accompanied by a decrease in the increment of the amount of martensite. This feature can be explained as follows. In accordance with (41), let the temperature that is optimum for the growth of packet martensite in pure iron be the M_s^I temperature of the first branch of the concentration dependence $M_s(C)$, to which a point close to (0.4, 0.4) corresponds in the plane of the variables T' and Γ' in (39). In the absence of the concentration contribution, the change in T corresponds to motion along the straight line $T' \approx \Gamma'(T)$ [with $a_0 \approx 2$ in (42)]. In the case of a fixed concentration C, the cooling and heating lead to a displacement of the figurative point along the straight line $T' \approx \Gamma'(T) - \Gamma'(C)$ that is parallel to the line $T' \approx \Gamma'(T)$. An increase in T' only weakly changes the level of the derivative $\partial f/\partial \mu'$, but a decrease in the magnitude of the overcooling relative to T_0 leads, first, to a decrease in the starting deformation and, second, to an increase in the threshold deformation, which necessarily decreases the time of growth of the lath crystal. With decreasing T, the decrease in σ_0/σ_{th} is caused by a rapid decrease in σ_0 due to the decrease in $\partial f/\partial \mu'$ for points lying below curve *2* in Fig. 11.

For the completeness of the analysis, we recall that at grain sizes exceeding the critical size, apart from the above-considered cooling-induced martensite, crystals of deformation-induced martensite can be formed (at the stage of plastic flow), which is related to the carriers of threshold deformation called crystons. The crystons (shear superdislocation carriers that arise upon the contact interaction of dislocations with intersecting slip planes) specify the orientations of habit planes during their propagation [139–141]. Figure 13 displays the formation scheme of a cryston due to the interaction of n and m dislocations with different initial slip systems. The cryston concept is also constructive in describing shear bands with an arbitrary crystallographic orientation of planar boundaries [142–144].

Figure 14 schematically shows the logical structure of the dynamic approach to the description of martensitic transformations.

The diffusionless spontaneous structural phase transformations (during cooling) in separate small particles and in grains of austenite polycrystals of size less than the critical size require an independent analysis. For example, in the nanocrystalline state (with the grain diameter $\leqslant 100$ nm), the martensitic transformation is either suppressed completely (e.g., in Fe–Ni alloys) or is modified (as in titanium nickelide-based alloys), losing the characteristics such as habit, which are inherent morphological signs of martensite in single crystals and in grains of size $D > D_c$. A typical feature is twinning in an ordered crystalline structure of the central regions of nanograins. It is obvious that the role of the most long-wavelength displacements now passes to natural oscillations of the grains and the maximum wavelength is now limited from below by the doubled grain diameter. In the chains of fine ($\leqslant 10$ nm) contacting grains, a reaction of the transformation of a grain as a whole is in principle possible, accompanied by a relay-type transfer of deformation from

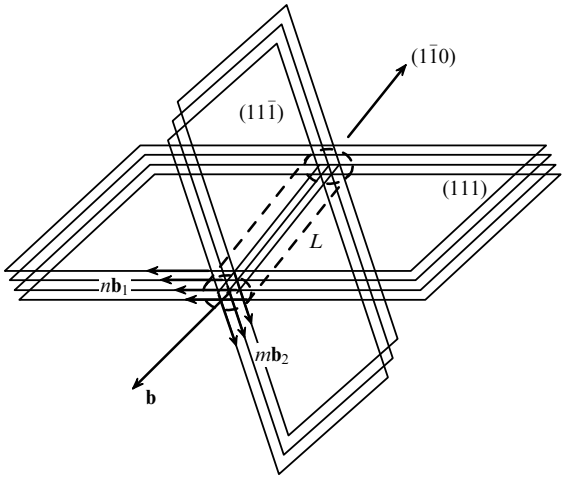

Figure 13. Generalized Frank–Read source (typical of the fcc phase) of crystons characterized by a total (superposition) Burgers vector $\mathbf{b} \| n\mathbf{b}_1 + m\mathbf{b}_2$.

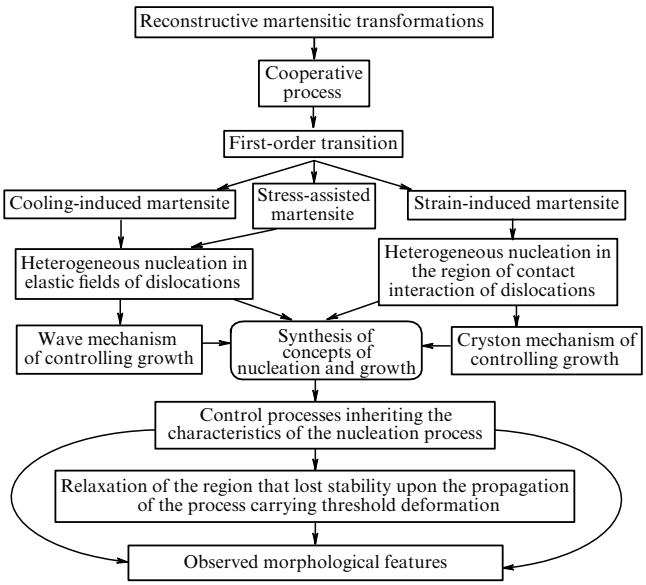

Figure 14. Key points of the description of a martensitic reaction in single crystals and in polycrystalline materials with the grain size exceeding the critical size D_c.

grain to grain. In [120], in a qualitative analysis of the possibility of the occurrence of a martensitic transformation in the nanocrystalline state, we called such an MT 'accommodational,' bearing in mind both the internal twinning accommodation and the above-mentioned intergrain relay-type accommodation. In Table 2, taken from [120], we give a characteristic hierarchy of the spatial scales. It can be seen that with decreasing the critical size of the structure, the role of the 'long-wavelength' displacement passes to the displacements that played the role of 'short-wavelength' displacements at the preceding scale level, which reflects the existing similarity in the dynamics of the martensitic reaction.

In the dynamical description of structural rearrangements in a nanocrystalline state, it seems natural to consider nonlinear excitations of the medium with an explicit account for its discrete nature [145]. It is obvious that nonlinear excitations (like breathers and kinks) with a wide spectrum of propagation velocities and a dynamic structure of concerted short-wavelength longitudinal and transverse displacements are capable of describing both the initial excited states and the various structural rearrangements (in particular, polytypic transformations related to regular reshufflings of planes) [120, 146]. An adequate dynamic picture can apparently also be obtained for the concept of a 'transformation dislocation' introduced into the phenomenological theory. This concept is actually used as a synonym of the transformation front, with whose propagation the lateral growth of crystals for the thermoelastic MT is usually associated [147]. It cannot be ruled out that the interpretation of polymorphic transformation as a reconstruction of coordination polyhedra (suggested in [148]) will occupy its niche in the dynamic picture of rearrangements on the nanoscale level. The success of this theory is to a significant extent due to taking the nonequilibrium state of the system into account. It is natural that the fundamental and constructive role of the nonequilibrium of the system is emphasized in describing the majority of deformation-related processes in [149].

Table 2. Hierarchy of typical critical grain sizes D_c, thicknesses of martensite crystals d, and twin thicknesses d_{tw}.

Martensite type	D_c	d	d_{tw}
Quenching and stress martensite	1 μm	10 – 100 nm	3 – 10 nm
Strain-induced martensite	0.1 μm	1 – 10 nm	
Accommodational twinned martensite	20 – 100 nm	20 – 100 nm	1 – 3 nm
Accommodational martensite of a single orientation. Transformation of a grain as a whole	3 – 10 nm	3 – 10 nm	

11. Conclusions

In making the final conclusions, we can state that the current model of the formation of a martensite crystal (including the stages of heterogeneous nucleation, wave growth, and accommodation of the coexisting phases) in the case of a spontaneous (in the process of cooling) $\gamma-\alpha$ martensitic transformation in iron alloys realized in single crystals or in polycrystals with grain sizes $D > D_c$ is generally complete. The high degree of the completeness of the description of the observed features of the transformation suggests a new paradigm of the dynamic theory of the spontaneous $\gamma-\alpha$ MT. This conclusion can also be related to the dynamic theory of the formation of stress-assisted martensite (upon cooling in an external elastic field), in which case we simply observe a reduction in the number of realized variants of orientations of martensite crystals (compared to that observed in the case of a spontaneous transformation).

The conformity of the theory to the observed picture of an MT is beyond doubt. This opens a wide field of activity for using the diverse tools of physical acoustics in the analysis of the morphological features of separate crystals (e.g., plate-like or wedge-like forms), their junctions (acute and obtuse), mutual intersections, interactions with grain boundaries, etc., on the basis of the concepts of the CWP as a superposition of wave beams propagating in metastable austenite and capable of disturbing its stability. In particular, the shapes of the profiles of martensite crystals formed in a medium containing planar inhomogeneities were analyzed in [150].

As regards other promising avenues of investigations, we note the possibility of extending the applicability of the theory to bcc–hcp and hcp–bcc transitions, which require an additional short-wavelength 'reshuffling' of planes (which does not affect the macroscopic morphological features), and to first-order transitions close to second order ones (e.g., in titanium nickelide-based alloys). Of unquestionable interest is also the refinement of the dynamic description of the accommodation MT in the nanocrystalline state.

References

1. Seljakow N, Kurdjumow G, Goodtzow N Z *Zh. Prikl. Fiz.* (4) 51 (1927); *Z. Phys.* **45** 384 (1927)
2. Kurdjumow G, Sachs G *Zh. Prikl. Fiz.* (9–10) 165 (1930); *Z. Phys.* **64** 325 (1930)
3. Nishiyama Z *Sci. Rep. Tohoku Imp. Univ.* **23** 637 (1934)
4. Greninger A B, Troiano A R *Metals Trans.* **185** 590 (1949)
5. Bunsha R F, Mehl R F *Trans. AIME* **197** 1251 (1953)
6. Lokshin F L *Nauch. Dokl. Vyssh. Shkoly* (2) 205 (1958)

7. Schastlivtsev V M, Kaletina Yu V, Fokina E A *Martensitnoe Prevrashchenie v Magnitnom Pole* (Martensitic Transformation in a Magnetic Field) (Ekaterinburg: UrO RAN, 2007)
8. Bain E C *Trans. AIME* **70** 25 (1924)
9. Kurdyumov G V, Utevskii L M, Entin R I *Prevrashcheniya v Zheleze i Stali* (Transformations in Iron and Steel) (Moscow: Nauka, 1977)
10. Wechsler M S, Lieberman D S, Read T A *Trans. AIME* **197** 1503 (1953)
11. Bowles J S, Mackenzie J K *Acta Metall.* **2** 129 (1954)
12. Mackenzie J K, Bowles J S *Acta Metall.* **2** 138 (1954)
13. Bowles J S, Mackenzie J K *Acta Metall.* **2** 224 (1954)
14. Barrett C S, Massalski T B *Structure of Metals* (Oxford: Pergamon, 1980) [Translated into Russian (Moscow: Metallurgiya, 1984)]
15. Landau L D, Lifshitz M *Statisticheskaya Fizika* Ch. I (Statistical Physics, Pt. 1) (Moscow: Nauka, 1976) [Translated into English (Oxford: Pergamon Press, 1980)]
16. Roitburd A L *Usp. Fiz. Nauk* **113** 69 (1974) [*Sov. Phys. Usp.* **17** 326 (1974)]
17. Hirth J P, Lothe J *Theory of Dislocations* (New York: McGraw-Hill, 1968) [Translated into Russian (Moscow: Atomizdat, 1972)]
18. Cottrell A H *Theory of Crystal Dislocations* (New York: Gordon and Breach, 1964) [Translated into Russian (Moscow: Mir, 1969)]
19. Kashchenko M P *Volnovaya Model' Rosta Martensita pri* γ–α *Prevrashchenii v Splavakh na Osnove Zheleza* (Wave Model of Martensite Growth upon the γ–α Transformation in Iron-Based Alloys) (Ekaterinburg: UIF Nauka, 1993)
20. Kashchenko M P "The wave model of martensite growth for the FCC-BCC transformation of iron-based alloys," cond-mat/0601569
21. Bilby B A, Christian J W, in *The Mechanism of Phase Transformations in Metals* (London: The Institute of Metals, 1956) p. 121 [Translated into Russian in *Usp. Fiz. Nauk* **70** 515 (1960)]
22. Wayman C M, in *Physical Metallurgy* Vol. 1 (Eds R W Cahn, P Haasen) 3rd ed. (Amsterdam: North-Holland, 1983) p. 1031 [Translated into Russian Vol. 2 (Moscow: Metallurgiya, 1987)]
23. Patashinskii A Z, Pokrovskii V L *Fluktuatsionnaya Teoriya Fazovykh Perekhodov* (Fluctuation Theory of Phase Transitions) (Moscow: Nauka, 1982) [Translated into English (Oxford: Pergamon Press, 1979)]
24. Falk F *Z. Phys. B* **51** 177 (1983)
25. Falk F *Z. Phys. B* **54** 159 (1984)
26. Barsch G R, Horovitz B, Krumhansl J A *Phys. Rev. Lett.* **59** 1251 (1987)
27. Bales G S, Gooding R J *Phys. Rev. Lett.* **67** 3412 (1991)
28. Saxena A et al. *J. Physique IV* **5** C8-125 (1995)
29. Rasmussen K Ø et al. *Phys. Rev. Lett.* **87** 055704 (2001); cond-mat/0001410
30. Reid A C E, Gooding R J *Phys. Rev. B* **50** 3588 (1994)
31. Rao M, Sengupta S *Phys. Rev. Lett.* **78** 2168 (1997)
32. Theil F, Levitas V I "A study of a hamiltonian model for phase transformations including microkinetic energy," patt-sol/9811006
33. Fischer F D "Mechanics and phase transformation," in *Advances in Mechanical Behaviour, Plasticity and Damage. Proc. of EUROMAT 2000* Vol. 1 (Eds D Miannay et al.) (Amsterdam: Elsevier, 2000) p. 41
34. Wang L X, Melnik R V N "Thermo-mechanical wave propagation in shape memory alloy rod with phase transformations," cond-mat/0702689
35. Lobodyuk V A, Estrin E I *Usp. Fiz. Nauk* **175** 745 (2005) [*Phys. Usp.* **48** 713 (2005)]
36. Serebryakov V G, Estrin E I *Dokl. Akad. Nauk SSSR* **237** 322 (1977) [*Sov. Phys. Dokl.* **22** 682 (1977)]
37. Krisement O, Houdremont E, Wever F *Rev. Metall.* **51** 401 (1954) [Translated into Russian in *Fazovye Prevrashcheniya v Stali* (Phase Transformations in Steel) (Moscow: Metallurgizdat, 1961)]
38. Mogutnov B M, Tomilin I A, Shvartsman L A *Termodinamika Zhelezo-Uglerodistykh Splavov* (Thermodynamics of Iron–Carbon Alloys) (Moscow: Metallurgiya, 1972)
39. Kaufman L, Cohen M, in *Progress in Metal Physics* Vol. 7 (Eds B Chalrmers, R King) (London: Pergamon Press, 1958) p. 165 [Translated into Russian in *Uspekhi Fiziki Metallov* Vol. 4 (Moscow: Metallurgizdat, 1961)]
40. Kashchenko M P, Vereshchagin V P *Fiz. Met. Metalloved.* **58** 450 (1984)
41. Vinnikov L Ya et al. *Metallofizika* **55** 24 (1974)
42. Sarrak V I, Suvorova S O *Izv. Akad. Nauk SSSR, Met.* (6) 90 (1982)
43. Machlin E S, Cohen M *Trans. AIME* **191** 1019 (1951)
44. Meyers M A *Acta Metall.* **28** 757 (1980)
45. Rabinovich M I, Trubetskov D I *Vvedenie v Teoriyu Kolebanii i Voln* (Oscillations and Waves in Linear and Nonlinear Systems) (Moscow: Nauka, 1984) [Translated into English (Dordrecht: Kluwer Academic, 1989)]
46. Wasilewski R J *Metall. Trans. A* **6** 1405 (1975)
47. Kayser U *J. Phys. F* **2** L60 (1972)
48. Zhang J *J. Phys. F* **14** 769 (1984)
49. Izotov V I, Khandarov P A *Fiz. Met. Metalloved.* **34** 332 (1972)
50. Hausch G, Warlimont H *Acta Metall.* **21** 401 (1973)
51. Delaey L et al., in *Proc. ICOMAT-79 Cambridge, Masachusets, USA, 24-29 June 1979*, p. 400
52. Hallman E D, Brockhouse B N *Can. J. Phys.* **47** 1117 (1969)
53. Endoh Y *J. Magn. Magn. Mater.* **10** 177 (1979)
54. Zverev V M, Silin V P, Preprint No. 1972-92 (Moscow: FIAN, 1972)
55. Zverev V M, Silin V P *Kratk. Soobshch. Fiz.* (6) 46 (1984)
56. Barsch G R, Krumhansl J A *Metall. Trans. A* **19** 761 (1988)
57. Isyumov Y A, Laptev V M, Syromyatnicov V N *Phase Transit.* **49** 1 (1994)
58. Van Tendeloo G, Chandrasekaran M, Lovey F C, in *Proc. ICOMAT-86, Intern. Conf. on Martensitic Transformations* (Sedai: Japan Institute of Metals, 1986) p. 868
59. Pushin V G, Kondrat'ev V V, Khachin V N *Predperekhodnye Yavleniya i Martensitnye Prevrashcheniya* (Pretransition Phenomena and Martensitic Transformations) (Ekaterinburg: UrO RAN, 1998)
60. Tyapkin Yu D et al. *Fiz. Met. Metalloved.* **41** 1040 (1976)
61. Kondrat'ev V V et al. *Fiz. Met. Metalloved.* **47** 102 (1979)
62. Izyumov Yu A, Syromyatnikov V N *Fazovye Perekhody i Simmetriya Kristallov* (Phase Transitions and Crystal Symmetry) (Moscow: Nauka, 1984) [Translated into English (Dordrecht: Kluwer Academic, 1990)]
63. Cech R E, Turnbull D *Trans. AIME* **206** 124 (1956)
64. Kashchenko M P, Vereshchagin V P *Izv. Vyssh. Uchebn. Zaved., Fiz.* (8) 16 (1989) [*Sov. Phys. J.* **32** 592 (1989)]
65. Kashchenko M P, Vereshchagin V P *Izv. Vyssh. Uchebn. Zaved., Fiz.* (8) 20 (1989) [*Sov. Phys. J.* **32** 596 (1989)]
66. Vereshchagin V P, Kashchenko M P *Fiz. Tverd. Tela* **33** 1605 (1991) [*Sov. Phys. Solid State* **33** 906 (1991)]
67. Vereshchagin V P, Kashchenko S M, Kashchenko M P *Izv. Vyssh. Uchebn. Zaved., Fiz.* (9) 79 (1991) [*Sov. Phys. J.* **34** 808 (1991)]
68. Kashchenko M P, Vereshchagin V P, Aristova N V *Fiz. Met. Metalloved.* **75** (2) 38 (1993) [*Phys. Met. Metallogr.* **75** 135 (1993)]
69. Vereshchagin V P, Kashchenko M P *Metalloved. Term. Obrab. Met.* (7) 6 (1994)
70. Letuchev V V, Konovalov S V, Kashchenko M P *J. Phys. IV* **5** C2-53 (1995)
71. Letuchev V V et al. *J. Phys. IV* **5** C8-151 (1995)
72. Konovalov S V, Yablonskaya T N, Kashchenko M P *Zh. Tekh. Fiz.* **66** (11) 177 (1996) [*Tech. Phys.* **41** 1181 (1996)]
73. Kashchenko M P et al. *Fiz. Met. Metalloved.* **83** (3) 43 (1997) [*Phys. Met. Metallogr.* **83** 237 (1997)]
74. Kashchenko M P et al. *Fiz. Met. Metalloved.* **85** (4) 25 (1998) [*Phys. Met. Metallogr.* **85** 392 (1998)]
75. Kashchenko M P, Mints R I *Fiz. Tverd. Tela* **19** 329 (1977)
76. Kashchenko M P *Fiz. Met. Metalloved.* **58** 862 (1984)
77. Kashchenko M P *Izv. Vyssh. Uchebn. Zaved., Fiz.* (3) 41 (1982) [*Sov. Phys. J.* **25** 229 (1982)]
78. Kashchenko P *Izv. Vyssh. Uchebn Zaved, Fiz.* (2) 7 (1982) [*Sov. Phys. J.* **25** 87 (1982)]
79. Fedorov F I *Teoriya Uprugikh Voln v Kristallakh* (Theory of Elastic Waves in Crystals) (Moscow: Nauka, 1965) [Translated into English (New York: Pergamon, 1968)]
80. Kashchenko M P et al. *Fiz. Met. Metalloved.* **76** 90 (1993) [*Phys. Met. Metallogr.* **76** 300 (1993)]
81. Kashchenko M P et al. *Izv. Akad. Nauk SSSR, Met.* (2) 105 (1992)
82. Kashchenko M P et al. *Fiz. Met. Metalloved.* (1) 146 (1992) [*Phys. Met. Metallogr.* **73** 48 (1992)]

83. Letuchev V V et al. *J. Mater. Sci. Lett.* **11** 1683 (1992)
84. Ziman J *Principles of the Theory of Solids* (Cambridge: Cambridge Univ. Press, 1972) [Translated into Russian (Moscow: Mir, 1974)]
85. Kashchenko M P, in *Martensitnye Prevrashcheniya v Metallakh i Splavakh* (Martensitic Transformations in Metals and Alloys), Dokl. Mezhdunarod. konf. 'I-77', Kiev, March 16–20, 1977 (Kiev: Naukova Dumka, 1978) p. 137
86. Kashchenko M P, Mints R I *Pis'ma Zh. Eksp. Teor. Fiz.* **26** 433 (1977) [*Sov. JETP Lett.* **26** 309 (1977)]
87. Kashchenko M P *Izv. Vyssh. Uchebn. Zaved., Fiz.* (3) 113 (1982)
88. Lax M "Fluctuation and coherent phenomena in classical and quantum physics," in *Statistical Physics, Phase Transitions and Superconductivity* Vol. 2 (Eds M Chretien, E P Gross, S Deser) (New York: Gordon and Breach, 1968) [Translated into Russian (Moscow: Mir, 1975)]
89. Kashchenko M P, Mints R I *Zh. Eksp. Teor. Fiz.* **75** 2280 (1978) [*Sov. Phys. JETP* **48** 1149 (1978)]
90. Kashchenko M P *Fiz. Met. Metalloved.* **49** 937 (1980)
91. Vereshchagin V P, Kashchenko M P *Fiz. Met. Metalloved.* **61** 237 (1986)
92. Kashchenko M P, Skorikova N A, Chashchina V G *Fiz. Met. Metalloved.* **99** (5) 3 (2005) [*Phys. Met. Metallogr.* **99** 447 (2005)]
93. Skorikova N A, Chashchina V G, Kashchenko M P *Izv Vyssh. Uchebn. Zaved., Fiz.,* (11) 44 (2005) [*Russ Phys. J.* **48** 1154 (2005)]
94. Kashchenko M P, Skorikova N A, Chashchina V G *Mater. Sci. Eng. A* **438 – 440** 99 (2006)
95. Kashchenko M P, Skorikova N A, Chashchina V G *Mater. Sci. Eng. A* **481 – 482** 201 (2008)
96. Kashchenko M P, Skorikova N A, Chashchina V G *Fiz. Met. Metalloved.* **106** (3) 229 (2008) [*Phys. Met. Metallogr.* **106** 219 (2008)]
97. Ziman J M *Electrons and Phonons* (Oxford: Clarendon Press, 1960) [Translated into Russian (Moscow: IL, 1962)]
98. Shtremel' M A *Prochnost' Splavov* Ch. 2 *Deformatsiya* (Strength of Alloys. Pt 2: Deformation) (Moscow: MISiS, 1997)
99. Kashchenko M P, Chashchina V G *Fizich. Mezomekh.* **13** (1) 29 (2010)
100. Naimark O B *Fizich. Mezomekh.* **11** (2) 89 (2008)
101. Blatt F J *Physics of Electronic Conduction in Solids* (New York: McGraw-Hill, 1968) [Translated into Russian (Moscow: Mir, 1971)]
102. Kashchenko M P, Chashchina V G *Fiz. Mezomekh.* (1) 37 (2010)
103. Kashchenko M P, Eishinskii E R *Fiz. Met. Metalloved.* **56** 681 (1983)
104. Mirzaev D A, Morozov O P, Shteinberg M M *Fiz. Met. Metalloved.* **36** 560 (1973)
105. Shteinberg M M, Mirzaev D A, Ponomareva T N *Fiz. Met. Metalloved.* **43** 166 (1977)
106. Mirzaev D A et al. *Fiz. Met. Metalloved.* **51** 364 (1981)
107. Mirzaev D A et al. *Fiz. Met. Metalloved.* **47** 125(1979)
108. Mirzaev D A *Fiz. Met. Metalloved.* **47** 986 (1979)
109. Scheil E *Z. Anorg. Chem.* **180** 1 (1929)
110. Umemoto M, Owen W S *Metall. Trans.* **5** 2041 (1974)
111. Knapp H, Dehlinger U *Acta Mettall.* **4** 289 (1956)
112. Gorbach V G, Pechkovskii E P, Trefilov V I *Ukr. Fiz. Zh.* **16** 133 (1971)
113. Pechkovskii E P, Trefilov V I , Preprint No. 71.4 (Kiev: Institute of Metal Physics, Akad. Nauk Ukr. SSR, 1971)
114. Solov'ev V A *Problemy Metallovedeniya i Fiziki Metallov* (Problems of Metallography and Metal Physics) (Moscow: Metallurgiya, 1976)
115. Gaidukov M G, Sadovskii V D *Dokl. Akad. Nauk SSSR* **96** 67 (1977)
116. Petrov Yu N *Defekty i Bezdiffuzionnoe Prevrashchenie v Stali* (Defects and the Diffusionless Transformation in Steel) (Kiev: Naukova Dumka, 1978)
117. Ivanov Yu F et al. *Zh. Tekh. Fiz.* **65** (3) 199 (1995) [*Tech. Phys.* **40** 278 (1995)]
118. Blinova E N et al. *Izv. Ross. Akad. Nauk, Ser. Fiz.* **65** 1444 (2001)
119. Glezer A L, Blinova E N, Pozdnyakov V A *Izv. Ross. Akad. Nauk, Ser. Fiz.* **66** 1263 (2002)
120. Kashchenko M P, Chashchina V G *Fundam. Probl. Sovrem. Materialoved.* **5** (2) 40 (2008)
121. Kashchenko M P, Chashchina V G, Vikharev S V *Izv. Vyssh. Uchebn. Zaved., Fiz.* (8) 94 (2009) [*Russ. Phys. J.* **52** 875 (2009)]
122. Kashchenko M P, Chaschina V G, Vikharev S V *Izv. Vyssh. Uchebn. Zaved., Fiz.* (9) 96 (2009) [*Russ. Phys. J.* **52** 997 (2009)]
123. Kashchenko M P, Chashchina V G, Vikharev S V *Fiz. Met. Metalloved.* **110** 212 (2010) [*Phys. Met. Metallogr.* **110** 200 (2010)]
124. Kashchenko M P, Chashchina V G, Vikharev S V *Fiz. Met. Metalloved.* **110** 323 (2010) [*Phys. Met. Metallogr.* **110** 305 (2010)]
125. Kashchenko M P, Chashchina V G *Dinamicheskaya Model' Formirovaniya Dvoinikovykh Martensitnykh Kristallov pri* γ–α *Prevrashchenii v Splavakh Zheleza* (Dynamic Model of the Formation of Twinned Martensitic Crystals upon γ– α Transformation in Iron Alloys) (Ekaterinburg: Ural. Gos. Lesotekh. Univ., 2009)
126. Kashchenko M P, Chashchina V G *Fiz. Met. Metalloved.* **105** 571 (2008) [*Phys. Met. Metallogr.* **105** 537 (2008)]
127. Kashchenko M P, Chashchina V G *Fiz. Met. Metalloved.* **106** 16 (2008) [*Phys. Met. Metallogr.* **106** 14 (2008)]
128. Kashchenko M P, Chashchina V G *Izv. Vyssh. Uchebn. Zaved., Fiz.* (7) 3 (2008) [*Russ. Phys. J.* **51** 659 (2008)]
129. Kashchenko M P, Chaschina V G *Izv. Vyssh. Uchebn. Zaved., Fiz.* (11) 42 (2008) [*Russ. Phys. J.* **51** 1161 (2008)]
130. Chaschina V G *Izv. Vyssh. Uchebn. Zaved., Fiz.* (7) 95 (2009) [*Russ. Phys. J.* **52** 766 (2009)]
131. Dunne D P, Bowles J S *Acta Metall.* **17** 201 (1969)
132. Krivoglaz M A et al. *Zakalka Stali v Magnitnom Pole* (Quenching of Steel in a Magnetic Field) (Moscow: Nauka, 1977)
133. Leont'ev A A, Schastlivtsev V M, Romashev L N *Fiz. Met. Metalloved.* **58** 950 (1984)
134. Kashchenko M P, Chashchina V G *Dinamicheskaya Model'* γ–α *Martensitnogo Prevrashcheniya v Splavakh Zheleza i Reshenie Problemy Kriticheskogo Razmera Zerna* (Dynamic Model of the γ–α Martensitic Transformation in Iron Alloys and the Solution of the Problem of the Critical Grain Size) (Moscow–Izhevsk: RKhD, Inst. Komp'yut. Issled., 2010)[1]
135. Kashchenko M P, Konovalov S V, Yablonskaya T N *Izv. Vyssh. Uchebn. Zaved., Fiz.* (6) 64 (1994) [*Russ. Phys. J.* **37** 567 (1994)]
136. Chashchina V G, Fedorovskikh E S, Kashchenko M P, in *Mezhdunarodnaya Nauchno-Tekhnicheskaya Shkola–Seminar* (International Research School–Seminar) (Ekaterinburg: UGTU–UPI, 2009) p. 428
137. Kashchenko M P, Chashchina V G, Konovalov S V *Materialoved. Term. Obrab. Mater.* (9) 44 (2010)
138. Rodionov D P, Schastlivtsev V M *Stal'nye Monokristally* (Steel Single Crystals) (Ekaterinburg: URO RAN, 1996)
139. Kashchenko M P, Semenovykh A G, Chashchina V G *Vopr. Materialoved.* (1) 253 (2002)
140. Kashchenko M P, Semenovih A G, Chashchina V G *J. Physique IV* **112** 147 (2003)
141. Kashchenko M P, Semenovykh A G, Chashchina V G *Fiz. Mezomekh.* **6** (3) 37 (2003)
142. Kashchenko M P, Chashchina V G, Semenovih A G, in *Advances in Mechanical Behaviour, Plasticity and Damage. Proc. of EUROMAT 2000* Vol. 1 (Eds D Miannay et al.) (Amsterdam: Elsevier, 2000) p. 305
143. Kashchenko M P, Semenovykh A G, Chashchina V G *Fiz. Mezomekh.* **6** (1) 95 (2003)
144. Kashchenko M P, Mal'tseva O A, Chashchina V G *Fiz. Met. Metalloved.* **99** (3) 98 (2005) [*Phys. Met. Metallogr.* **99** 314 (2005)]
145. Bebikhov Yu V, Dmitriev S V, Khare A *Fundam. Probl. Sovrem. Materialoved.* **6** (3) 55 (2009)
146. Chashchina V G *Izv. Vyssh. Uchebn. Zaved., Fiz.* (7) 92 (2009) [*Russ. Phys. J.* **52** 763 (2009)]
147. Malygin G A *Usp. Fiz. Nauk* **171** 187 (2001) [*Phys. Usp.* **44** 173 (2001)]
148. Kraposhin V S *Probl. Chern. Metall. Materialoved.* (1) 62 (2008)
149. Panin V E, Egorushkin V E *Fiz. Mezomekh.* **11** (2) 9 (2008)
150. Chashchina V, Kashchenko M, Vikharev S "Wave model of forming of the martensite crystal in the heterogeneity medium," arXiv:1003.2952

[1] Monographs [125, 134] and the second edition of [19] are freely available on the site http://kashchenko.com.